6-1995

Three Nonhomogeneous Poisson Models for the Probability of Basaltic Volcanism: Application to the Yucca Mountain Region, Nevada

Charles B. Connor
Southwest Research Institute, cbconnor@usf.edu

Brittain E. Hill
Southwest Research Institute

Three nonhomogeneous Poisson models for the probability of basaltic volcanism:
Application to the Yucca Mountain region, Nevada

Charles B. Connor and Brittain E. Hill

Center for Nuclear Waste Regulatory Analyses, Southwest Research Institute, San Antonio, Texas

Abstract. The distribution and timing of areal basaltic volcanism are modeled using three nonhomogeneous methods: spatio-temporal nearest neighbor, kernel, and nearest-neighbor kernel. These models give nonparametric estimates of spatial or spatio-temporal recurrence rate based on the positions and ages of cinder cones and related vent structures and can account for migration and shifts in locus, volcano clustering, and development of regional vent alignments. The three methods are advantageous because (1) recurrence rate and probability maps can be made, facilitating comparison with other geological information; (2) the need to define areas or zones of volcanic activity, required in homogeneous approaches, is eliminated; and (3) the impact of uncertainty in the timing and distribution of individual events is particularly easy to assess. The models are applied to the Yucca Mountain region (YMR), Nevada, the site of a proposed high-level radioactive waste repository. Application of the Hopkins F test, Clark-Evans test, and K function indicates volcanoes cluster in the YMR at the >95% confidence level. Weighted-centroid cluster analysis indicates that Plio-Quaternary volcanoes are distributed in four clusters: three of these clusters include cinder cones formed <1 Ma. Probability of disruption within the 8 km^2 area of the proposed repository by formation of a new basaltic vent is calculated to be between 1×10^{-4} and 5×10^{-4} in 10^4 years (the kernel and nearest-neighbor kernel methods give a maximum probability of 5×10^{-4} in 10^4 years), assuming regional recurrence rates of 5–10 volcanoes/m.y. An additional finding, illustrating the strength of nonhomogeneous methods, is that maps of the probability of volcanic eruption for the YMR indicate the proposed repository lies on a steep probability gradient: volcanism recurrence rate varies by more than 2 orders of magnitude within 20 km. Insight into this spatial scale of probability variation is a distinct benefit of application of these methods to hazard analysis in areal volcanic fields.

Introduction

The distribution and timing of volcanism in areal basaltic volcanic fields have been the focus of numerous studies, primarily with the aim of better understanding the processes that govern magma supply and the role of crustal structure in influencing magma ascent [*Settle*, 1979; *Nakamura*, 1977; *Wadge and Cross*, 1988; *Connor*, 1990; *Lutz and Gutmann*, 1995]. Three basic aspects of cinder cone distribution have been described through these and related studies: (1) shifts in the locus of cinder cone volcanism are a common phenomenon in volcanic fields; (2) cinder cones cluster within these fields, often on several scales; and (3) vent alignments are ubiquitous, including short local alignments of several vents and more regional alignments that are usually more than 20 km in length and consist of numerous vents. Patterns in the distribution and timing of basaltic volcanism also have been used to assess hazards. For example, *Wadge et al.* [1994] made a quantitative analysis of the distribution of lava boccas on Mount Etna as part of their assessment of lava flow hazards.

Here, three spatial and spatio-temporal nearest-neighbor

models are presented to describe areal patterns in basaltic volcanism. These models are applied to the probability of volcanic eruption occurring in the Yucca Mountain region (YMR), Nevada. This approach features several characteristics of nearest-neighbor methods which make them amenable to volcano distribution studies and hazard analysis in areal volcanic fields. First, volcanic eruptions, such as the formation of a new cinder cone, are discrete in time and space. Using nearest-neighbor methods, the probability surface is estimated directly from the location and timing of these past, discrete volcanic events. As a result, nearest-neighbor models are sensitive to the patterns generally recognized in cinder cone distributions. Furthermore, the resulting probability surfaces are continuous, rather than consisting of abrupt changes in probability that must be introduced in spatially homogeneous models. Continuous probability surfaces can be readily compared to other geologic data, such as fault location, that may influence volcano distribution. Nearest-neighbor methods also eliminate the need to define areas or zones of volcanic activity as is required by all spatially homogeneous Poisson models. Finally, uncertainties in the ages of individual volcanic events and the distribution of Neogene volcanoes are important limitations on the usefulness of all probability approaches. The impact of these uncertainties in the timing and distribu-
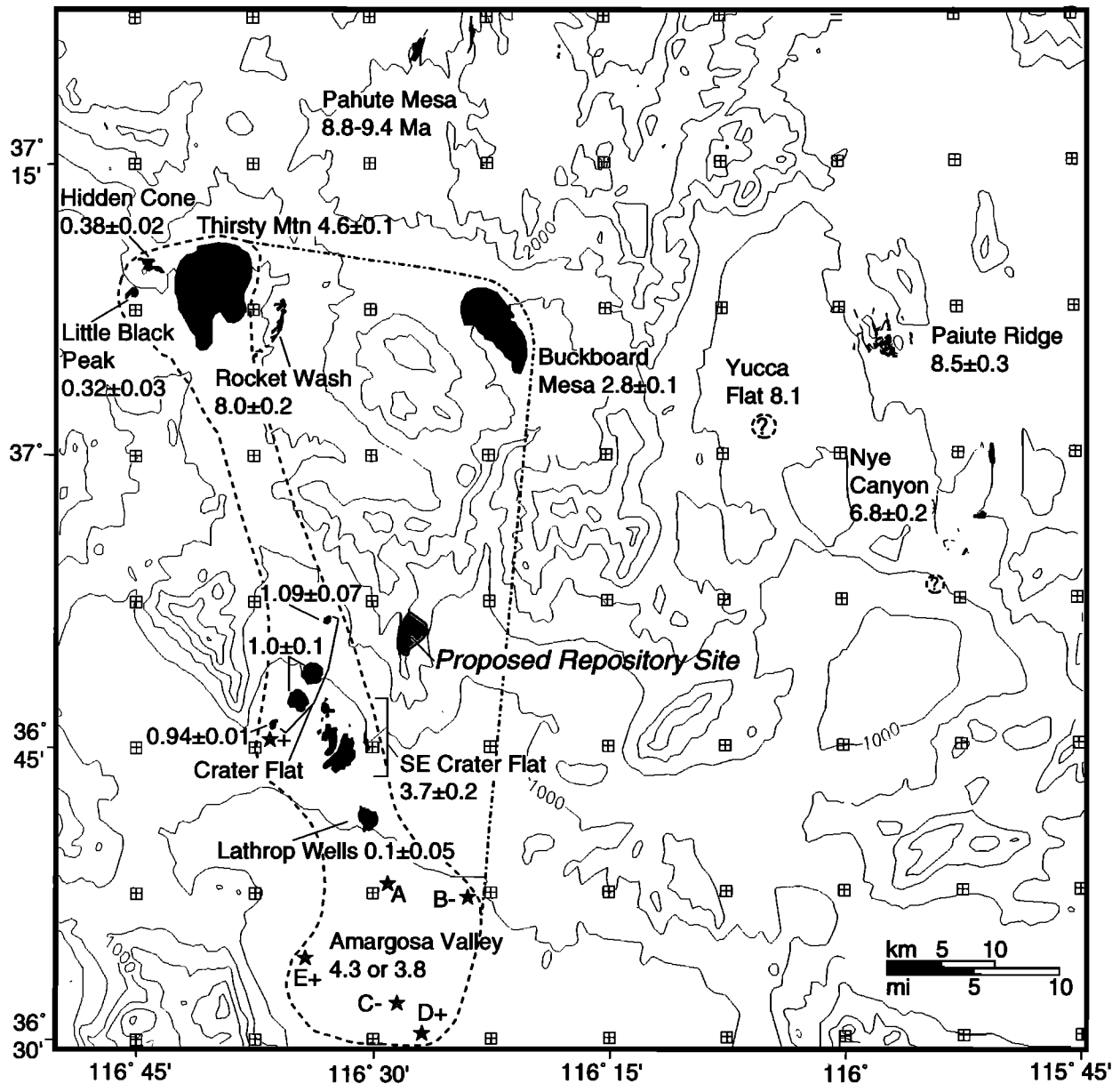
Figure 1. Basaltic vents, lavas, and intrusions of the Yucca Mountain region (YMR) younger than about 9 Ma. Geology compiled from *Byers et al.* [1966]; *Ekren et al.* [1966]; *Carr and Quinlivan* [1966]; *Byers and Barnes* [1967]; *Byers and Cummings* [1967]; *Hinrichs et al.* [1967]; *Noble et al.* [1967]; *Tschanz and Pampeyan* [1970]; *Cornwall* [1972]; *Crowe et al.* [1983, 1986]; *Carr* [1984]; *Swadley and Carr* [1987]; and *Faulds et al.* [1994]. Locations of aeromagnetic anomalies (stars) from *Kane and Bracken* [1983] and *Langenheim et al.* [1993]. Sources for age estimates are listed in Table 1. Dashed line is the Crater Flat Volcanic Zone (CFVZ) [*Crowe and Perry*, 1989], dashed-dotted line is the area of most recent volcanism (AMRV) [*Smith et al.*, 1990]. Contours generated from regional a 3-arc-sec digital elevation model, 200-m contour interval. Universal transverse mercator projection, Nevada zone 11, North American Datum 1983.

tion of individual events is relatively easy to assess using nearest-neighbor models.

Basaltic volcanism in the YMR has been the topic of numerous previous studies focusing on the probability of volcanic disruption of a proposed high-level radioactive waste repository [*Crowe et al.*, 1982; *Ho*, 1991; *Ho et al.*, 1991; *Crowe et al.*, 1992a; *Sheridan*, 1992]. These studies are pursued largely because the proposed waste repository is located within 10–20 km of at least five Quaternary cinder cones (Figure 1) and the high-level radioactive waste must be

isolated from the surrounding environment for a period of at least 10,000 years. Most models assessing the probability of future volcanism in the YMR and the likelihood of a repos-itory-disrupting event rely on the assumption that Plio-Quaternary basaltic volcanoes are distributed in a spatially uniform random manner over some bounded area [e.g., *Crowe et al.*, 1982, 1992a; *Ho et al.*, 1991; *Margulies et al.*, 1992]. However, as in many other volcanic fields, patterns in the distribution and age of basaltic volcanoes in the YMR make the choice of these bounded areas somewhat subjec-

tive. Spatial variations in the YMR volcanic field are shown by shifts in the locus of basaltic volcanism from east to west since the cessation of caldera-forming volcanism in the Miocene Southern Nevada Volcanic Field [*Crowe and Perry*, 1989]. *Crowe et al.* [1992a] and *Sheridan* [1992] also noted that basaltic vents appear to cluster in the YMR. *Sheridan* [1992] suggests that one parametric method of accounting for spatial heterogeneity in vent distribution is to assume that post-4 Ma volcanoes located close to the proposed repository are formed as a result of steady state activity and that the dispersion of these vents represents two standard deviations on an elliptical Gaussian probability surface. Using this assumption, *Sheridan* [1992] modeled the probability of repository disruption by Monte Carlo simulation for both volcanic events and dike intrusions, noting that variations in the shape of the probability surface significantly alter the probability of igneous disruption of the proposed repository. An alternative approach used to assess volcanic hazards in the YMR has been to define specific areas in which the recurrence rate of igneous events is increased. *Smith et al.* [1990] and *Ho* [1992] define NNE trending zones within which average recurrence rates exceed that of the surrounding region. These zones correspond to cinder cone alignment orientations that *Smith et al.* [1990] and *Ho* [1992] hypothesize may occur as a result of structural control. The objectives of our application of nearest-neighbor methods in the YMR are (1) to account for observed heterogeneities in volcano distribution in our estimate of the probability of volcanism in the area and within the boundaries of the proposed repository; (2) to use these methods to map variation in probability of volcanism across the region for the first time, thus placing the probability of volcanic eruption occurring at or near the repository in a more regional context; and (3) to compare the three nearest-neighbor estimates, and previous estimates, of the probability of volcanic eruption in the area.

Patterns in Cinder Cone Volcanism

Patterns in the distribution and timing of cinder cone volcanism in the YMR are similar to patterns identified in other, often more voluminous volcanic fields. For example, shifts or migration in the location of volcanism over periods of millions of years have been documented in many basaltic volcanic fields. In the Coso Volcanic Field, California, *Duffield et al.* [1980] found that basaltic volcanism has taken place in essentially two stages. Eruption of basalts occurred over a broad area in what is now the northern and western portions of the Coso Volcanic Field from approximately 4 to 2.5 Ma. In the Quaternary the locus of volcanism shifted to the southern portion of the Coso field. *Condit et al.* [1989] noted the tendency for basaltic volcanism to gradually migrate from west to east in the Springerville Volcanic Field between 2.5 and 0.3 Ma. Other examples of continental basaltic volcanic fields in which the location of cinder cone volcanism has migrated include the San Francisco Volcanic Field, Arizona [*Tanaka et al.*, 1986], the Lunar Crater Volcanic Field, Nevada [*Foland and Bergman*, 1992], the Michoacán-Guanajuato Volcanic Field, Mexico [*Hasenaka and Carmichael*, 1985], and the Cima Volcanic Field, California [*Dohrenwend et al.*, 1984; *Turrin et al.*, 1985]. In some areas, such as the San Francisco and Springerville Volcanic Fields, migration is readily explained by plate movement

[*Tanaka et al.*, 1986; *Condit et al.*, 1989; *Connor et al.*, 1992]. In other areas the direction of migration or shifts in the locus of volcanism does not correlate with the direction of plate movement. In either case, models developed to describe the recurrence rate of volcanism or to predict locations of future eruptions in volcanic fields need to be sensitive to these shifts in the location of volcanic activity.

On a slightly finer scale, cinder cones are known to cluster within many volcanic fields [*Heming*, 1980; *Hasenaka and Carmichael*, 1985; *Tanaka et al.*, 1986]. Spatial clustering can be recognized through field observation, or through the use of exploratory data analysis or cluster analysis techniques [*Connor*, 1990]. Clusters identified using the latter approach in the Michoacán-Guanajuato and the Springerville Volcanic Fields were found to consist of 10-100 individual cinder cones. Clusters in these fields are roughly circular to elongate in shape with diameters of 10-50 km. The simplest explanation for the occurrence, size, and geochemical differences between many of these clusters is that these areas have higher magma supply rates from the mantle. Factors affecting magma pathways through the upper crust, such as fault distribution, appear to have little influence on cluster formation [*Connor*, 1990; *Connor and Condit*, 1994]. In some volcanic fields, such as Coso, the presence of silicic magma bodies in the crust may influence cinder cone distribution by impeding the rise of denser mafic magma [*Eichelberger and Gooley*, 1977; *Bacon*, 1982], resulting in the formation of mafic volcano clusters peripheral to the silicic magma bodies.

Tectonic setting, strain rate, and fault distribution all may influence the distribution of basaltic vents within clusters, and sometimes across whole volcanic fields [*Nakamura*, 1977; *Smith et al.*, 1990; *Parsons and Thompson*, 1991; *Takada*, 1994]. *Kear* [1964] discussed local vent alignments, in which vents are the same age and easily explained by a single episode of dike injection, and regional alignments, in which vents of varying age and composition are aligned over distances of 20-50 km or more. Numerous mathematical techniques have been developed to identify and map vent alignments on different scales, including the Hough transform [*Wadge and Cross*, 1988], two-point azimuth analysis [*Lutz*, 1986], and frequency domain map filtering techniques [*Connor*, 1990]. Regional alignments identified using these techniques are commonly colinear or parallel to mapped regional structures. For example, *Draper et al.* [1994] mapped vent alignments in the San Francisco Volcanic Field which are parallel to, or colinear with, segments of major fault systems in the area. About 30% of the cinder cones and maars in the San Francisco Volcanic Field are located along these regional alignments [*Draper et al.*, 1994]. *Lutz and Gutmann* [1995] identified similar patterns in the Pinacate Volcanic Field, Mexico. Although alignments can clearly form due to episodes of dike injection [*Nakamura*, 1977] and therefore are sensitive to stress orientation [*Zoback*, 1989], there are also examples of injection along preexisting faults [e.g., *Kear*, 1964; *Draper et al.*, 1994] oblique to maximum horizontal compressional stress.

Cumulatively, these studies indicate that models describing the recurrence rate, or probability, of basaltic volcanism should reflect the clustered nature of basaltic volcanism and shifts in the locus of basaltic volcanism through time. Models also should be amenable to comparison with basic geological data, such as fault patterns and neotectonic stress

information, which may impact vent distributions on a comparatively more detailed scale. In addition, probability models should incorporate uncertainties in the distribution and timing of volcanism. Uncertainty in the distribution of volcanoes is particularly important for Neogene volcanoes. These volcanoes may be buried as a result of subsequent volcanic activity [e.g., Condit et al., 1989] or sedimentation [e.g., Langenheim et al., 1993], or have been so deeply eroded that vent locations can not be recognized. Uncertainty in the ages of volcanoes is due to variations in the precision and accuracy of different techniques used to date volcanic events and to open-system movement of radiogenic components.

Finally, it is possible to define a volcanic event in various ways. A simple definition that can be applied to young cinder cones, spatter mounds, and maars is based on morphology: an individual edifice represents an individual volcanic event. Volcanic events used in distribution analyses are commonly defined as mapped vents [Condit et al., 1989; Connor et al., 1992; Lutz and Gutmann, 1995; Wadge et al., 1994], or volcanic edifices of a minimum size [Hasenaka and Carmichael, 1985; Connor, 1990; Bemis and Smith, 1993]. In older, eroded systems, evidence for the occurrence of vents, such as near-vent breccias or radial dikes, is required. However, several edifices can form in single, essentially continuous, eruptive episodes. For example, three closely spaced cinder cones formed during the 1975 Tolbachik fissure eruption [Tokarev, 1983; Magus'kin et al., 1983]. In this case, the three cinder cones represent a single eruptive event that is distributed over a larger area than is represented by a single cinder cone. The three 1975 Tolbachik cinder cones have very different morphologies and erupted adjacent to three older (late? Holocene) cinder cones [Braytseva et al., 1983]. Together this group forms a 5-km-long north trending alignment. Without observing the formation of this alignment, it likely would be difficult to resolve the number of volcanic events represented by these six cones. This type of eruptive activity results in uncertainty in the number of volcanic events represented by individual cones, even where these vents are well-preserved.

These uncertainties represent a serious problem in most, if not all volcanic fields, because often there is no clear way to resolve them. An alternative approach is to ascertain the impact of these uncertainties on the probability model. This approach is adopted by developing several data sets for basaltic volcanism in the YMR that likely bound the uncertainties associated with the age, distribution, and number of volcanic events in the area.

Modeling Vent Distribution

Aherne and Diggle [1978] define two measures of intensity (expected number of points (i.e., volcanoes) per unit area):

$$\lambda_p = m \left/ \sum_{i=1}^{m} u_i \right. \tag{1}$$

$$\lambda_v = m \left/ \sum_{i=1}^{m} v_i \right. \tag{2}$$

where u_i and v_i are areas of circles whose radii are the distance from the ith randomly chosen point to the nearest

volcano, and the ith volcano to its nearest neighbor, respectively; m is the number of nearest neighbors and in this case is equal to the number of volcanoes; λ_p is the intensity estimated from m point-to-volcano measurements; and λ_v is the intensity estimated from m volcano-to-volcano measurements. *Aherne and Diggle* [1978] used these measures of intensity to distinguish between homogeneous Poisson point distributions, for which λ_p and λ_v should be approximately equal, and clustered distributions, for which λ_v tends to measure the intensity within clusters and λ_p is a measure of cluster intensity [Ripley, 1981]. The Hopkins F test [Ripley, 1981] uses the ratio

$$\mathrm{Hop}_F = \lambda_p / \lambda_v \tag{3}$$

tested against a Fisher $F(2m, 2m)$ distribution [Byth and Ripley, 1980], the null hypothesis being that $\mathrm{Hop}_F = 1$ and volcanoes have a homogeneous Poisson distribution. Assuming that some area can be identified in which all points, p, are located, Hop_F provides one means of distinguishing clustered and random volcano distributions. Numerous similar tests exist, including the Clark and Evans [1955] test and the K function [Ripley, 1977]. Calculation of these statistics, coupled with a spatial cluster analysis [Späth, 1980; Connor, 1990], provides an effective means of characterizing the spatial distribution of volcanoes.

The expected recurrence rate per unit area [Diggle, 1977; 1978; Ripley, 1977; 1981; Cressie, 1991] must be estimated in most volcanic fields because clustering causes a marked departure of recurrence rate per unit area from the average recurrence rate. Here, three nearest-neighbor estimates of recurrence rate and their assumptions are described. All three methods are nonparametric, and the recurrence rate estimates are controlled by the distribution and timing of past volcanism.

Method 1: Spatio-temporal Nearest-Neighbor Estimate

The first method provides a spatial and temporal estimate of recurrence rate:

$$\lambda_n(x, y) = m \left/ \sum_{i=1}^{m} u_i t_i \right. \tag{4}$$

where nearest-neighbor volcanoes are determined as the minimum $u_i t_i$, t_i is the time elapsed since the formation of the ith nearest-neighbor volcano, and u_i is defined as before (equation (1)), with $u_i \geq 1$ km^2.

The relationship between this estimate of recurrence rate and homogeneous Poisson models, in which the recurrence rate is a constant over time and within a specified area, can be illustrated by describing the behavior of $\lambda_n(x, y)$ when a completely spatially and temporally random process is sampled. Modifying (4) slightly,

$$z_i = u_i t_i \tag{5}$$

$$\lambda_n(x, y) = m \left/ \sum_{i=1}^{m} z_i = 1/E(Z) \right. \tag{6}$$

where $E(Z)$ is the expected value of z. If volcanoes form as the result of a completely spatially and temporally random process, $E(Z)$ can be thought of as the expected time and

area within which n volcanoes will form and z must have a gamma density distribution [*Ripley*, 1981]. Therefore the probability density function for z is

$$f_z(z) = \frac{\lambda^n}{(n-1)!} z^{n-1} e^{-\lambda z} \qquad (7)$$

where λ is the average recurrence rate within some specified area and over some specified time interval. The expected value of z, given this probability density function, becomes

$$E(Z) = \frac{\lambda^n}{(n-1)!} \int_0^\infty z^n e^{-\lambda z} \, dz \qquad (8)$$

$$E(Z) = \frac{\lambda^n}{(n-1)!} \frac{n!}{\lambda^{n+1}} = \frac{n}{\lambda}. \qquad (9)$$

In order to compare $E(Z)$ with the recurrence rate per unit area, as defined in (6), $E(Z)$ is evaluated for $n = 1$, that is, the expected time and area within which one new volcano will form. Combining (6) and (9),

$$\lambda_n(x, y) = \lambda \qquad (10)$$

for completely spatially and temporally random distributions. The nearest-neighbor estimate of recurrence rate $\lambda_n(x, y)$ becomes a constant equal to the average recurrence rate over some specified area if the underlying distribution is completely spatially and temporally random. This nearest-neighbor nonhomogeneous Poisson model thus is simply a general form of homogeneous Poisson models. One distinct advantage of using the more general nearest-neighbor nonhomogeneous Poisson models rather than homogeneous Poisson models is that regions within which λ is taken to be constant need not be defined.

Therefore it is reasonable to compare the expected regional recurrence rate calculated using various nearest-neighbors (equation (4)):

$$\lambda_t = \int_X \int_Y \lambda_n(x, y) \, dy \, dx \qquad (11)$$

with the observed regional recurrence rate. In practice, recurrence rates $\lambda_n(x, y)$ are calculated on a grid and these values are summed over the region of interest:

$$\lambda_t = \sum_{i=0}^{q} \sum_{j=0}^{n} \lambda_n(i, j) \Delta x \Delta y \qquad (12)$$

where in this case, Δx and Δy are the grid spacing used in the calculations and q and n are the number of grid points used in the X and Y directions, respectively.

Summarizing the first method, several assumptions are made in the application of (4) to estimate the intensity of volcanism and the probability of volcanic eruption in a particular volcanic field. The most important assumption is that the appropriate number of nearest-neighbor volcanoes can be estimated from the regional recurrence rate. In areas of concentrated volcanism, such as the Springerville Volcanic Field, the frequency of vent-forming eruptions is high enough to make recurrence rate estimates fairly straightforward [*Connor and Condit*, 1994]. In other areas, such as the

YMR, greater uncertainty exists in recurrence rate estimates because of the comparatively small number of events [*Crowe et al.*, 1982; *Ho et al.*, 1991]. In addition, the use of (4) assumes that u_i and t_i have been adequately determined for each volcano. Here, t_i is taken to represent the time since the formation of the volcano. Finally, it is assumed that each volcano is adequately represented as a point. However, as described below, various area terms may be used to alleviate this assumption. In practice, it is relatively simple to test the sensitivity of the model results to both uncertainty in the ages of volcanoes and estimates of the regional recurrence rate of volcanism by computing the recurrence rate using a range of parameters.

Method 2: Kernel Estimate

Lutz and Gutmann [1995] applied a kernel method [*Silverman*, 1986] for estimation of the spatial recurrence rate of volcanism in their study of vent alignment distribution in the Pinacate Volcanic Field. In the kernel estimation technique, spatial variation in estimated recurrence rate is a function of distance to nearby volcanoes and a smoothing constant h. The kernel function is a probability density function which is symmetric about the locations of individual volcanoes. Following the example of *Lutz and Gutmann* [1995], an Epanechnikov kernel is used [*Cressie*, 1991]. For a purely spatial, bivariate distribution

$$\begin{aligned} \kappa_i &= (2/\pi)[1 - (d_i/h)^2], \quad (d_i/h)^2 < 1, \\ \kappa_i &= 0, \quad \text{otherwise} \end{aligned} \qquad (13)$$

where h is the smoothing constant used to normalize the distance d_i between the location for which recurrence rate is estimated and the ith volcano. The spatial recurrence rate at point (x, y) is then

$$\lambda_h(x, y) = \frac{1}{e_h} \sum_{i=1}^{n} h^{-2} \kappa_i \qquad (14)$$

where n volcanoes are used in the analysis and e_h is an edge correction [*Diggle*, 1985; *Cressie*, 1991]. In the case of a volcanic field, integrating $\lambda_h(x, y)$ over some large area A relative to the size of the field and the smoothing constant, h, should yield n. Therefore, if $e_h = n$, then

$$\int_A \lambda_h(x, y) \, da = 1,$$

where the units of $\lambda_h(x, y)$ are volcanoes per square kilometer. Using this value for e_h, $\lambda_h(x, y)$ can be multiplied by an estimate of the temporal recurrence rate λ_t to calculate the expected number of volcanoes per unit area per time. The value of $\lambda_h(x, y)$ at a given point (x, y) depends on the number of volcanoes found within a distance h of the point. If no volcanoes are located within h of the point, then $\lambda_h(x, y) = 0$.

Eruptions will have a high probability close to existing volcanoes if h is chosen to be small. Conversely, a large value of h will result in a more uniform probability distribution. Clearly, utility of the kernel model depends on the assumption that the smoothing constant can be estimated in a geologically meaningful way. *Silverman* [1986] recommends using a wide range of smoothing constants in density

calculations, an approach adopted by *Lutz and Gutmann* [1995]. An identical approach is used here. However, the range of reasonable smoothing constants is further constrained by using a spatial cluster analysis. The shape of the kernel function is an additional assumption in the model. Alternative kernel functions include uniform random and normal density distributions. Although *Cressie* [1991] and *Lutz and Gutmann* [1995] indicate that the choice of the kernel function is not as important as the choice of an appropriate smoothing constant, we used several different kernels in our analysis of volcano distribution in the YMR. Even with this limited number of volcanic events, we also found that the kernel function has a trivial impact on probability calculations compared with the choice of a smoothing constant.

Method 3: Nearest-Neighbor Kernel Estimate

In method 3 a value $r_m(x, y)$ is substituted for the smoothing constant, h, in (14), where $r_m(x, y)$ is the distance between point (x, y) and the mth nearest-neighbor volcano [*Silverman*, 1986]. In this case, the nearest-neighbor is determined on the basis of distance only, rather than using the measure $u_i t_i$ used in method 1. For $m \geq 1$, $\lambda_r(x, y) > 0$ everywhere. Thus this nearest-neighbor kernel method produces smoother variation in the probability surface than is calculated for all but the largest values of a smoothing constant in method 2. Nonetheless, the estimated recurrence rate will be higher near the center of clusters than is estimated using the large values for the smoothing constant in method 2. As in method 1, the number of nearest neighbors used to estimate $\lambda_r(x, y)$ will strongly impact the results and experimentation using a range of nearest neighbors is necessary to identify the resulting variation in $\lambda_r(x, y)$. Unlike method 2, e_h will not always equal n in application of the nearest-neighbor kernel method [*Silverman*, 1986]. The simplest approach to determination of e_h is to first integrate estimates of $\lambda_r(x, y)$ over the entire region using $e_h = n$, then chose a value of e_h such that

$$\int_A \lambda_r(x, y) \, da = 1.$$

The value of e_h typically varies from $0.9n$ to n when estimated using this approach.

The three methods yield three different measures of recurrence rate, which are distinguished by subscript (method 1, $\lambda_n(x, y)$; method 2, $\lambda_h(x, y)$; method 3, $\lambda_r(x, y)$). Commonality between the three methods lies in the fact that each method depends fundamentally on the distribution of past volcanic events in order to estimate the probable locations of future volcanism. In the case of methods 1 and 3 the m nearest-neighbor volcanoes are used, defined by the distance to, or distance to and time since, past eruptions in the area. In method 2, only nearby volcanoes are used in the estimate of recurrence rate, where "nearby" is defined by the smoothing constant. Furthermore, in all three methods the calculation of a probability of future volcanism at a given location within a volcanic field depends on an estimate of the regional recurrence rate λ_t which is generally not known with certainty [*McBirney*, 1992; *Ho*, 1991].

Application to the Yucca Mountain Region

The proposed geological repository for high-level radioactive waste at Yucca Mountain, Nevada, provides one example of the increasing need to evaluate hazards due to areal basaltic volcanism. The objective of the repository is to isolate high-level radioactive waste from the accessible environment for at least the next 10,000 years, through deep (about 300 m) burial in Tertiary ignimbrites situated in the unsaturated zone several hundred meters above the local water table [*Department of Energy (DOE)*, 1988]. Volcanic eruptions at or near the repository could potentially release high-level radioactive waste into the accessible environment [*DOE*, 1988]. Therefore, determining the probability of a volcanic eruption in the repository area during the next 10,000 years is an important step in evaluating the potential risks associated with the Yucca Mountain site. The nearest-neighbor models described above provide one means of calculating these probabilities and evaluating their uncertainties.

Basaltic Volcanism in the Yucca Mountain Area

The YMR contains more than 30 late Miocene to Quaternary basaltic volcanoes distributed over approximately 2500 km². The region has been the site of recurring basaltic volcanism since the cessation of late Miocene caldera-forming activity in the Southwestern Nevada Volcanic Field [e.g., *Sawyer et al.*, 1994]. Basalts younger than about 9 Ma appear petrogenetically distinct from older basalts and better represent the mafic system that produced Quaternary eruptions in the YMR [*Crowe et al.*, 1983, 1986]. Figure 1 illustrates the location of mapped and inferred basaltic vents younger than about 9 Ma. Several subdivisions have been proposed for YMR postcaldera basaltic volcanism. The Crater Flat Volcanic Zone (CFVZ) of *Crowe and Perry* [1989] is a NNW trending zone that includes all YMR Quaternary volcanoes, most Pliocene volcanoes, and the Amargosa Valley aeromagnetic anomalies. The area of most recent volcanism (AMRV) of *Smith et al.* [1990] includes all Pliocene and younger YMR volcanoes. Both the CFVZ and AMRV are expanded from their original boundaries to include all of the aeromagnetic anomalies of Amargosa Valley [*Langenheim et al.*, 1993].

Vent locations in Table 1 were generally reported as such on geologic maps and in reports [*Byers et al.*, 1966; *Ekren et al.*, 1966; *Carr and Quinlivan*, 1966; *Byers and Barnes*, 1967; *Byers and Cummings*, 1967; *Hinrichs et al.*, 1967; *Noble et al.*, 1967; *Tschanz and Pampeyan*, 1970; *Cornwall*, 1972; *Crowe and Perry*, 1991; *Crowe et al.*, 1983, 1986, 1988; *Carr*, 1984; *Swadley and Carr*, 1987; *Faulds et al.*, 1994] or interpreted in the field from the presence of feeder dikes, vent agglutinate, or cinder cone remnants. Some of the Miocene volcanic centers have been eroded to hundreds of meters below the paleosurface, removing most of the evidence for vent locations. The number of vents reported for Pliocene and older volcanic centers should be regarded as a minimum estimate. Difficulty in recognizing older volcanic vents may impact estimated cluster size, shape, and longevity but has little impact on spatial or spatio-temporal recurrence rates when data are weighted by age.

Over 200 isotopic age determinations have been published for YMR basaltic rocks younger than about 9 Ma. Many of the older analyses have relatively low degrees of precision and are occasionally inaccurate. For example, dates as old as 10.4 ± 0.4 Ma are reported for the basalt of Pahute Mesa [*Crowe et al.*, 1983], which overlies the 9.40 ± 0.03 Ma Rocket Wash Tuff [*Sawyer et al.*, 1994]. Following the

Table 1. Data Used in the Analyses

Volcano (Abbreviation)	UTM Coordinate	Age Estimate, Ma	Source	Explanation	Data Set 1, Ma	Data Set 2, Ma
		Quaternary				
Hidden Cone (hc)	523230E 4112530N	0.38 ± 0.02	*Turrin* [1992]	Ar/Ar step heating, one sample	0.36	0.4
Little Black Peak (lb)	522130E 4110340N	0.32 ± 0.03	R. J. Fleck et al. (unpublished manuscript, 1994)	K-Ar, best estimated age from four measurements	0.29	0.35
Northern Cone (nc)	540330E 4079130N	1.09 ± 0.07	*Faulds et al.* [1994]	K-Ar on plagioclase separate, one sample; reversed magnetic polarity	1.02	1.16
Black Cone (bc)	538840E 4073990N	1.0 ± 0.1 0.71 ± 0.06	*Perry* [1994] *Faulds et al.* [1994]	Ar/Ar, average of four samples K-Ar on plagioclase separates, one sample; reversed magnetic polarity	0.78	1.1
Red Cone (rc)	537450E 4071470N	1.0 ± 0.1	*Faulds et al.* [1994]	K-Ar on plagioclase separates, average of three samples; reversed magnetic polarity	0.90	1.1
Little Cone NE (lcne)	535500E 4069490N	0.77 ± 0.04	*Faulds et al.* [1994]	K-Ar on plagioclase separate, one sample; reversed magnetic polarity	0.78	⋯
Little Cone SW (lcsw)	535131E 4069220N	0.94 ± 0.01 0.77 ± 0.04	*Heizler et al.* [1994] *Faulds et al.* [1994]	Ar/Ar step heating of sanidine xenocyrsts, one sample K-Ar on plagioclase separate, one sample; reversed magnetic polarity	0.78	0.94
Lathrop Wells (lw)	543780E 4060380N	0.1 ± 0.05	*Crowe et al.* [1992b], *Zreda et al.* [1993], *Poths et al.* [1994], and *Turrin et al.* [1991]	U/Th series and Ar/Ar dates generally >100 ka, ^{36}Cl and ^{3}He cosmogenic exposure dates generally <90 ka	0.05	0.15
		Pliocene				
Buckboard Mesa (bb)	554680E 4108970N	2.87 ± 0.06	R. J. Fleck et al. (unpublished manuscript, 1994)	K/Ar, best estimated age from four samples	2.8	2.9
Buckboard Mesa SE (bbse)	556060E 4107580N	2.87 ± 0.06		assumed to correlate with main Buckboard Mesa vent	2.8	⋯
Crater Flat A (cfa)	540232E 4071610N	3.7 ± 0.2	*Perry* [1994]	average of three Ar/Ar step-heating measurements, for undifferentiated Pliocene Crater Flat; all events in Pliocene Crater Flat are assumed to be relatively synchronous based on paleomagnetic work by *Champion* [1991]	3.5	3.9
Crater Flat B (cfb)	540330E 4070050N	3.7 ± 0.2			3.5	3.9
Crater Flat C (cfc)	540365E 4068790N	3.7 ± 0.2			3.5	3.9
Crater Flat D (cfd)	540696E 4067830N	3.7 ± 0.2			3.5	3.9
Crater Flat E (cfe)	540300E 4068390N	3.7 ± 0.2			3.5	⋯
Crater Flat F (cff)	540660E 4067470N	3.7 ± 0.2			3.5	⋯
Amargosa Valley B (avb)	553720E 4052990N	4.3 ± 0.1 3.8 ± 0.1	*Turrin* [1992] *Perry* [1994]	aeromagnetic anomaly [*Langenheim et al.*, 1993]; drilled and dated by Ar/Ar step heating; reversed magnetic polarity	3.7	4.3
Amargosa Valley A (ava)	546130E 4054260N	3.8 ± 0.1		aeromagnetic anomaly [*Langenheim et al.*, 1993], not drilled; assumed to correlate with anomaly B	3.7	⋯
Amargosa Valley E (ave)	538300E 4047200N	3.8 ± 0.1		aeromagnetic anomaly [*Langenheim et al.*, 1993], not drilled; assumed to correlate roughly with anomaly B; normal polarity	3.8	⋯

Table 1. (continued)

Volcano (Abbreviation)	UTM Coordinate	Age Estimate, Ma	Source	Explanation	Data Set 1, Ma	Data Set 2, Ma
		Pliocene				
Amargosa Valley C (avc)	547050E 4042950N	3.8 ± 0.1		aeromagnetic anomaly [*Langenheim et al.*, 1993], not drilled; assumed to correlate roughly with anomaly B; reversed polarity	3.7	...
Amargosa Valley D (avd)	549430E 4040080N	4.3 ± 0.1 3.8 ± 0.1		aeromagnetic anomaly, not drilled; assumed to correlate roughly with anomaly B; normal polarity; basalt found in nearby well [*Langenheim et al.*, 1993]	3.8	4.4
Thirsty Mountain (tm)	529390E 4112330N	4.6 ± 0.1	R. J. Fleck et al. (unpublished manuscript, 1994)	K/Ar estimate based on three samples	4.5	4.7
		Miocene				
Rocket Wash	536110E 4109120N	8.0 ± 0.2	*Crowe et al.* [1983]	K/Ar date	7.8	8.2
Pahute Mesa A	548920E 4133270N	9.8 ± 0.8	*Crowe et al.* [1983] and *Sawyer et al.* [1994]	overlies 9.40 ± 0.03 Pahute Mesa Member of Thirsty Canyon Tuff, two K/Ar dates	9.0	9.4
Pahute Mesa B	554090E 4135430N	8.8 ± 0.1	*Crowe et al.* [1983]	single K/Ar date	8.7	8.9
Pahute Mesa C	562370E 4132680N	9.8 ± 0.8	*Crowe et al.* [1983]	correlative with Pahute Mesa A	9.0	9.4
Paiute Ridge A	594860E 4107970N	8.5 ± 0.3	*Crowe et al.* [1983]	average of three K/Ar dates, undifferentiated Paiute Ridge; vent locations marked by exposed vent breccia, feeder dikes, or cone remnants	8.3	8.8
Paiute Ridge B	595780E 4106340N	8.5 ± 0.3			8.3	8.8
Paiute Ridge C	592810E 4105890N	8.5 ± 0.3			8.3	8.8
Paiute Ridge D	593411E 4105540N	8.5 ± 0.3			8.3	8.8
Paiute Ridge E	591480E 4105170N	8.5 ± 0.3			8.3	8.8
Nye Canyon A	603230E 4095790N	6.8 ± 0.2	*Crowe et al.* [1983]	average of three K/Ar dates, for undifferentiated Nye Canyon	6.6	7.0
Nye Canyon B	602170E 4088960N	6.8 ± 0.2			6.6	7.0
Nye Canyon C	600950E 4085920N	6.8 ± 0.2			6.6	7.0
Nye Canyon D	600550E 4085450N	6.8 ± 0.2			6.6	...
Nye Canyon E	599160E 4085820N	6.8 ± 0.2			6.6	...
Nye Canyon F	598030E 4090090N	6.8 ± 0.2			6.6	7.0
Nye Canyon G	597930E 4082470N	6.8 ± 0.2	*Carr* [1984]	drill hole in Frenchman Flat, assumed correlation with Nye Canyon	6.6	7.0
Yucca Flat	577860E 4093930N	8.1 ± 0.3	*Carr* [1984]	basalt in drill holes UE1h, UE1j, and UE6d; one K/Ar date	7.8	8.4

UTM, universal transverse mercator.

example of *Crowe* [1994], age estimates reported in Table 1 were selected from more recent analyses, which are generally regarded as more precise and accurate than older analyses [*Sinnock and Easterling*, 1983; *Vaniman and Crowe*, 1981; *Vaniman et al.*, 1982]. For units with multiple analyses the age estimates represent the mean and one standard deviation of the data set, and in cases where there is apparent discrepancy between two recent dates, both are incorporated in the analyses.

Several of the age estimates reported in Table 1 require

further explanation. The dipolar aeromagnetic anomalies in Amargosa Valley [*Kane and Bracken*, 1983; *Langenheim et al.*, 1993] have both normal (Figure 1, sites D and E) or reversed (Figure 1, sites B and C) magnetic polarities. Anomaly B has been drilled and samples of this basalt dated at 4.3 ± 0.1 [*Turrin*, 1992] and 3.8 ± 0.1 Ma [*Perry*, 1994]. Magnetic polarities are used to constrain the ages of the other anomalies, which have not been drilled but are interpreted to be caused by buried basaltic centers [*Langenheim et al.*, 1993]. The aeromagnetic anomaly in southern Crater Flat (Figure 1) likely represents a buried basalt with normal magnetic polarity [*Kane and Bracken*, 1983; *Crowe et al.*, 1986]. The age of this unit is problematic, as all of the other basalts in Crater Flat have reversed magnetic polarities [*Crowe et al.*, 1986]. This possible volcanic center is not included in our analyses. Over 100 age determinations are published for the Lathrop Wells volcano, which range from about 0.4 Ma to younger than 0.01 Ma and represent numerous analytical methods such as $^{40}Ar/^{39}Ar$ [*Turrin et al.*, 1991], U series disequilibrium [*Crowe et al.*, 1992b], and cosmogenic isotopes [*Poths and Crowe*, 1992; *Zreda et al.*, 1993; *Poths et al.*, 1994]. In an attempt to encompass many of the higher-precision age determinations for Lathrop Wells, we use an estimated age of 0.1 ± 0.05 for this volcano. A posteriori experimentation indicates that the age of Lathrop Wells may vary from 0.01 to 0.4 Ma with little impact on the probability of establishing a new volcano at the location of the repository.

Data Used in Models

On the basis of the abundant geological and geochronological data available for the YMR, we use two data sets throughout the following analyses. These two data sets are meant to encompass most of the uncertainty in the number and timing of volcanoes formed in the YMR. Data set 1 (Table 1) maximizes the number of events in the YMR. For example, closely spaced cinder cones, like Little Cone NE and Little Cone SW are treated as distinct events in data set 1. Furthermore, minimum ages are used in data set 1. These minimum ages are defined by the one-sigma uncertainty reported for age determinations. In cases where there is no overlap between two recent age determinations, such as is the case for Black Cone (Table 1), we use the younger of the dates in data set 1. Data set 2 excludes several mapped vents from the analysis because these vents are closely spaced and therefore may represent a single eruptive event. For example, Little Cone NE is not included in data set 2 because of its proximity to Little Cone SW. Also, several undrilled aeromagnetic anomalies are not included in data set 2. Older volcano ages are used in data set 2 (Table 1). These two data sets bound current estimates of the timing and distribution of postcaldera basaltic volcanic events in the YMR, noting that alternative data sets may certainly be developed and ages may be revised as additional geochronological analyses are published.

The type of event modeled using these two data sets is formation of a new volcano. Individual cones, isolated lava boccas, or mappable remnants of these structures represent events. In data set 1 these events include the construction of any Quaternary edifice by volcanic eruption. In data set 2, events include individual cones and cone pairs separated by <1 km. Events in this data set imply that vent pairs may be fed by the same intrusions at shallow levels during an

eruption. *Champion* [1991] has argued that the Quaternary Crater Flat alignment and similar cone alignments in the area formed during single episodes of volcanism. Thus all five cones in the Quaternary Crater Flat alignment may represent one eruptive event. One way to think of the two data sets is that they weight episodes of alignment formation by the number of volcanoes formed in each. This approach is consistent with the use of spatially nonhomogeneous models.

These two data sets are not appropriate for modeling the probability of reactivation of an existing cinder cone, a process that some investigators have suggested occurs in the YMR [e.g., *Wells et al.*, 1990; *Bradshaw and Smith*, 1994]. The probability models in this paper are used to determine the probability of formation of a new volcano, a spatial or spatio-temporal process. Reactivation of an existing vent is essentially a temporal process and should be modeled accordingly.

In addition, these two data sets are further divided by volcano age throughout the analyses that follow. Each analysis is made for all volcanoes in the data set (i.e., all mapped postcaldera basalts), volcanoes less than 5 Ma, and volcanoes less than 2 Ma. This is done in recognition of the nonstationary character of YMR cinder cone volcanism. Inspection of Figure 1, for example, reveals that late Miocene clusters have little spatial relationship to Pliocene and Quaternary cluster distribution [*Crowe and Perry*, 1989]. However, most Pliocene clusters have reactivated in the Quaternary. Thus further division of the two data sets preferentially weights the distribution of younger volcanoes.

Estimate of the regional recurrence rate of new volcano formation, λ_t, in the YMR during the Quaternary has received a great deal of study. These estimates range from about one volcano per million years (v/m.y.) to 8 v/m.y. [e.g., *Ho*, 1991; *Ho et al.*, 1991; *Crowe et al.*, 1992a]. This range of estimates is based on the application of various averaging techniques and statistical estimators. For example, one approach has been to consider that 7–8 volcanoes have formed in the last 1.8 m.y., yielding $\lambda_t \approx 4$ v/m.y. [*Crowe et al.*, 1982]. However, the YMR Quaternary volcanoes are all less than approximately 1 Ma, so averaging over the last one million years, $\lambda_t \approx 7$–8 v/m.y. For all postcaldera basalts, $\lambda_t \approx 3$ v/m.y. Using a maximum likelihood estimator, *Ho et al.* [1991] calculated $\lambda_t \approx 5$–6 v/m.y. Finally, on the basis of a Poisson-Weibull model, *Ho* [1992] calculated that $\lambda_t \approx 2$–13 v/m.y. with 90% confidence. We do not attempt to refine these estimates here. Rather, our probability estimates assume $\lambda_t = 5$–10 v/m.y. This range encompasses the known recurrence rate of volcano formation over the last 1 m.y. and allows for some variation about this value.

Probability Models

As a first step in analysis of volcano distribution in the YMR, the presence of volcano clusters is tested using data sets 1 and 2 (Table 1) and equations (1) and (2). Random points within the AMRV are used to calculate volcano intensity, λ_p (equation (1)). The value of λ_p may change depending on the position of the m random points. So, λ_p and Hop_F are calculated averaging the results of 100 simulations [*Cressie*, 1991] and reported with the standard error on the mean. Considering all volcanoes in the AMRV (i.e., data set 1), $Hop_F = 2.6 \pm 0.1$. Considering only Quater-
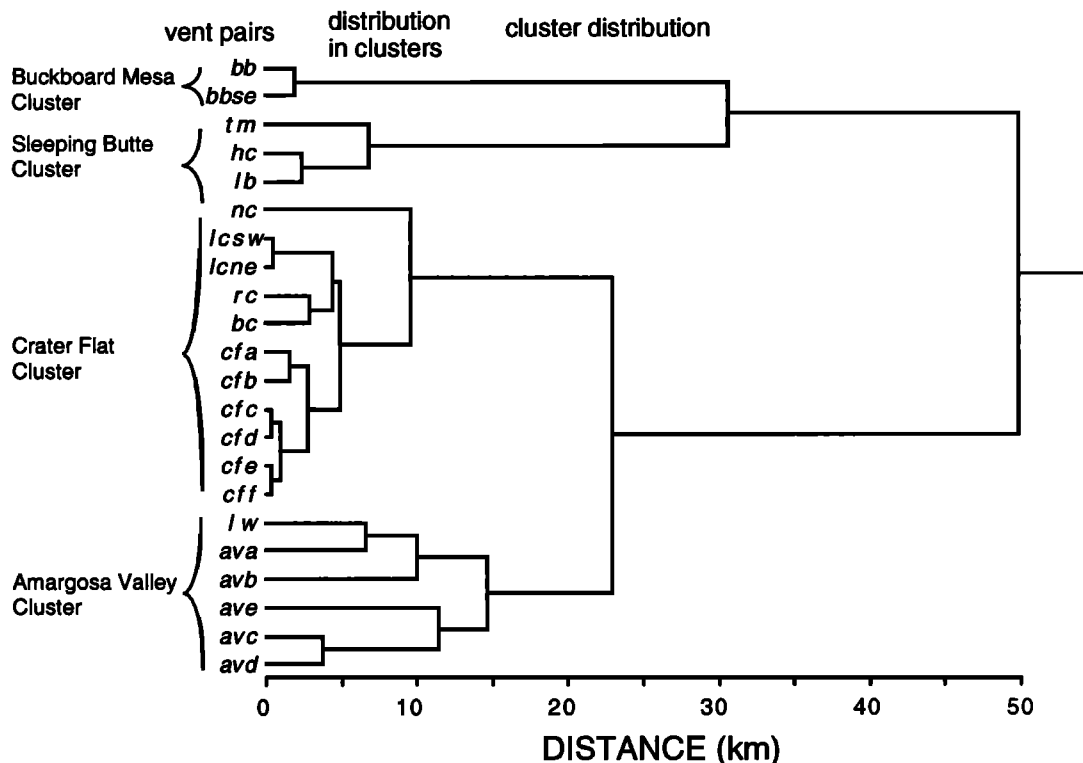
Figure 2. Weighted-centroid cluster analysis of volcano distribution in the YMR, calculated using data set 1 (Table 1) and volcanoes less than 5 Ma. Vent pairs group at distances of less than 2 km, clusters are completely formed at linkage distances of 15 km or less, and clusters begin to group at distances of greater than 23 km. Volcano abbreviations are given in Table 1.

nary volcanoes within the AMRV (data set 2), Hop_F = 7.1 ± 0.3. In either case, the null hypothesis that volcanoes are randomly distributed in the AMRV is rejected with greater than 95% confidence. Hopkins F test may be applied to smaller regions also. The CFVZ (Figure 1) is approximately 70 km long and 20 km wide and is a minimum area which includes Quaternary cinder cones of the YMR and the Amargosa Valley vents. Even using areas as small as the CFVZ, Hop_F = 3.1 ± 0.2 (data set 1) and clustering is significant with greater than 95% confidence. Application of similar measures of clustering, including the Clark-Evans test [Clark and Evans, 1955] and the K function [Ripley, 1977] shows that volcanoes in these areas are not randomly distributed at similar confidence levels. Consequently, we conclude that the recurrence rate of volcanism varies across the YMR, and therefore application of nearest-neighbor estimates of spatial and spatio-temporal variation in recurrence rate is appropriate.

A weighted-centroid cluster analysis [Späth, 1980] of vent distribution in the YMR helps illustrate vent clustering and provides additional insight into vent distribution. The results of the cluster analysis are shown by a dendrogram (Figure 2), which plots the distance at which individual cones and cluster centers link [Späth, 1980]. The dendrogram shown was calculated using data set 1 and volcanoes less than 5 Ma. The cluster analysis was repeated using both data sets, subdivided by age and a variety of clustering algorithms, with very similar results to those plotted (Figure 2).

The dendrogram shows that volcanoes form pairs and then larger clusters at short linkage distances. Cluster member-

ship changes rapidly until a linkage distance of 15 km, at which point four clusters occur. These are named the Amargosa Valley Cluster, including Lathrop Wells; the Crater Flat Cluster; Sleeping Butte Cluster, including Hidden Cone; Little Black Peak, and Thirsty Mountain (Figure 1); and the Buckboard Mesa Cluster, which consists of only two closely spaced vents. Each of these four clusters are complete and self-contained at linkage distances of 15 km or less and do not group with other clusters until linkage distances of ≥23 km, comparatively large changes in linkage distances. At 23 km the Amargosa Valley and Crater Flat Valley Clusters form a single group (Figure 2). Together these volcanoes are isolated from the Sleeping Butte and Buckboard Mesa Clusters. The Amargosa Valley and Crater Flat Clusters are less distinct using a single linkage clustering algorithm because of the comparatively intermediate position of Lathrop Wells (Figure 1).

Vent pairs that are grouped as single events in data set 2, such as the Little Cones, link at distances of less than 1 km. The absence of these vent pairs in the Amargosa Valley Cluster is evident comparing linkage distances in this cluster with Crater Flat. This may indicate the comparatively low resolution of aeromagnetic methods for the delineation of buried vent pairs or reflect a difference in the style of volcanism between the two clusters.

Adding a hypothetical volcanic event at the location of the candidate repository (Figure 1) alters the cluster analysis very little. The hypothetical repository event links with Northern Cone at a distance of 8.2 km; this group then links

with the rest of the Crater Flat Cluster at a distance of approximately 11 km.

In summary, the analysis of volcano distribution yields several observations that are useful for interpretation of the nearest-neighbor analyses. First, vents form statistically significant clusters in the YMR. Spatially, volcanoes less than 5 Ma form four clusters, the Crater Flat and Amargosa Valley Clusters overlapping somewhat due to the position of Lathrop Wells volcano and aeromagnetic anomaly A. Second, a volcanic event located at the repository would be spatially part of, albeit near the edge of, the Crater Flat Cluster, rather than forming between or far from clusters in the YMR. Third, three of the four clusters contain Quaternary basalt, indicating that these clusters are long-lived and provide some indication of the likely areas of future volcanism. Finally, the cluster analysis provides one means of estimating the smoothing constant h used in method 2. If h is chosen to be less than 15 km, then significant, perhaps unwarranted, variation in recurrence rate will be predicted within clusters. If h is chosen to be greater than 25–30 km, recurrence rate will be comparatively high between clusters. Choosing h between 15 and 25 km therefore will best capture the clustered nature of volcano distribution in the YMR.

Application of method 1. Regional recurrence rate is calculated using (3) and then compared with expected regional recurrence rate λ_t using (12). The calculations are repeated using the two data sets, further subdivided by age (Figure 3). For data set 1, 6 to 11 nearest-neighbor volcanoes give regional recurrence rates of 5–10 v/m.y. Data set 2 models this range of recurrence rates with 6–8 nearest-neighbor volcanoes. Limiting the analysis to younger volcanoes results in lower regional recurrence rates at a given number of nearest neighbors because Quaternary volcanoes are tightly clustered. Ten to thirteen nearest-neighbor volcanoes are required to model recurrence rates similar to the estimated postcaldera recurrence rate of <4 v/m.y.

In (7) the gamma density distribution was introduced to determine the expected time and area over which a new volcano will form. The Poisson distribution is used to determine the number of volcanoes that can be expected to
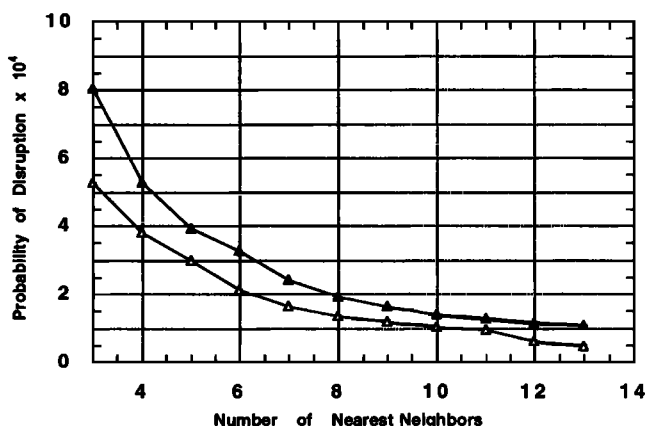
Figure 4. Estimated probability of disruption of the potential repository site, calculated using method 1, varies with the number of nearest neighbors used in the nonhomogeneous model. Calculations are made for the probability of a volcano forming within an 8 km^2 block at the Yucca Mountain repository site (Figure 1), during the next 10,000 years, using data set 1 (solid triangles) and data set 2 (open triangles). Each curve is calculated by solving equation (4) for $m = 3$ to 13 nearest-neighbor volcanoes, then using this value of $\lambda_n(x, y)$ to calculate probability at the repository (equation (16)). Different m nearest neighbors correspond to different regional recurrence rates λ_t (Figure 3).

form over a given time and area. In this case the probability of one or more volcanoes, $P[N(t) \geq 1]$, is of interest. The probability of volcanic disruption of the potential repository site is calculated for various estimates of $\lambda_n(x, y)$ (equation (4)),

$$P[N(t) \geq 1] = 1 - \exp\left[-t \int_X \int_Y \lambda_n(x, y) \, dy \, dx\right] \quad (15)$$

where the limits of integration define the area of the repository. This relation is closely approximated in discretized form

$$P[N(t) \geq 1] = 1 - \exp\left[-t \sum_a \lambda_n(x, y)\Delta x\Delta y\right], \quad (16)$$

where Δx and Δy each are 1 km and a is the area within which a volcanic eruption may occur and intersect the repository. These probabilities are very close to the probability of one volcanic event because the probability of two or more events is vanishingly small ($P[N(10,000 \text{ years}) > 1] \approx 1 \times 10^{-9}$), although it is noted that a single event using data set 2 may form more than one volcanic vent. Note that independence of events is always assumed in the application of the Poisson distribution. Because there is significant variation in $\lambda_n(x, y)$ and other estimates of recurrence rate of volcano formation across the region, the area $\Delta x \cdot \Delta y$ and time interval t must be small enough to be reasonably assured of independence. The application of (15) and (16) assumes that $\lambda_n(x, y)$ does not vary in a significant way within the area $\Delta x \cdot \Delta y$ or over the time interval t.

The probabilities of volcanic disruption of the repository using a range of nearest-neighbor models are given in Figure 4, calculated of $t = 10,000$ years and $a = 8$ km^2. The area
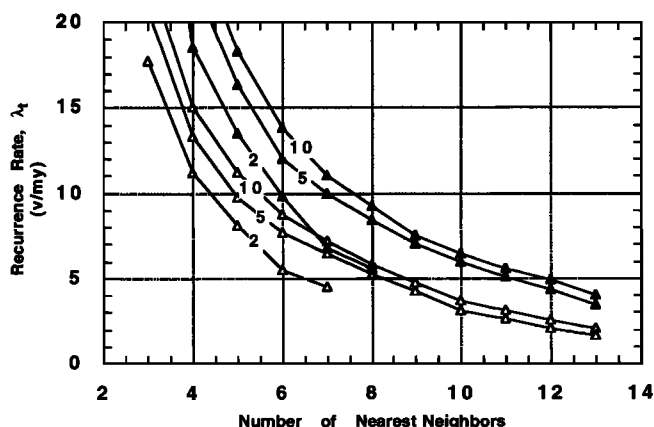

Figure 3. Recurrence rate for the formation of new volcanoes in the YMR is estimated using method 1 (equations (4) and (12)), calculated using data from Table 1. Solid triangles, data set 1; open triangles, data set 2. These data sets are further subdivided and calculations repeated for all volcanoes <10 Ma, <5 Ma, and <2 Ma.
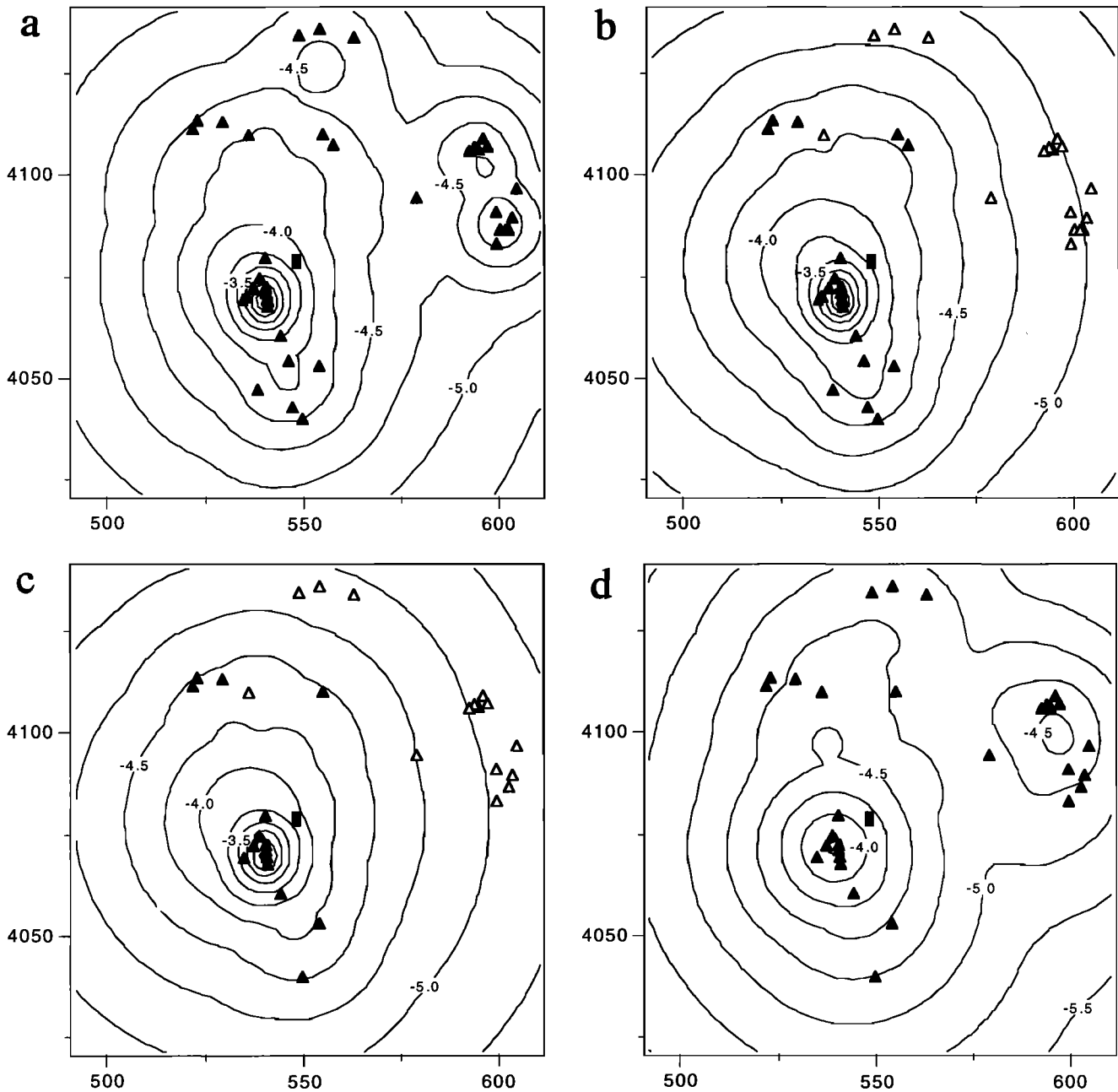
Figure 5. Probability of a new volcano forming during the next 10,000 years varies in the YMR because of the tendency for volcanoes to cluster. Here the logarithm of probability of a volcano forming within a 8 km² area during the next 10,000 years is contoured using (a) nine nearest neighbors and all volcanoes in data set 1, (b) eight nearest neighbors and all volcanoes in data set 1 formed <5 Ma, (c) seven nearest neighbors and all volcanoes in data set 2 formed <5 Ma, and (d) 11 nearest neighbors and all volcanoes in data set 2 formed <10 Ma. The four maps reflect different regional recurrence rates λ_t (Figure 3), ranging from $\lambda_t = 3$ v/m.y. (Figure 5d) to $\lambda_t = 8.5$ v/m.y. (Figure 5a). In these and all of the following maps, the solid triangles indicate the positions of volcanoes used in the calculation (data set 1 or 2), and open triangles indicate the positions of volcanoes that are part of the data set but are not included in the calculation because of their age. The location of the proposed repository (solid rectangle) is indicated. The contour interval is 0.25 log ($P[N \geq 1$, 10,000 years]) (e.g., -4 is a probability of 1×10^{-4} of a new volcano forming within an 8 km² area in 10,000 years). Map coordinates are in universal transverse mercator, North American Datum 1983.

of the actual repository is currently undetermined but is estimated to be approximately 6 km². Larger area terms (i.e., 8 km²) are presented to indicate the effects of an increase in repository size and, more importantly, to account

for the subsurface area directly affected by the emplacement of a new volcanic center. For example, emplacement of a cinder cone 500 m outside the repository boundary may result in dike injection within the repository itself. Using λ_t

= 5–10 v/m.y., $a = 8$ km^2, and both data sets in Table 1, the probability of disruption during a 10,000-year isolation period is between 9.0×10^{-5} and 3.3×10^{-4} (Figure 4). Altering the area term a from 6 to 10 km^2 has little impact on these probabilities. The probability of volcanic disruption of the proposed repository is greater than 1×10^{-4} for all but the lowest proposed values of λ_t (<3 v/m.y.).

One way to illustrate spatial variation in estimated recurrence rate in the YMR, and hence the probability of volcanic eruption, is to map probabilities calculated from nonhomogeneous Poisson models. Applying (4), the expected recurrence rate is estimated at points on a grid (grid node spacing of 2 km) using varying numbers of nearest neighbors. Probabilities of at least one event occurring within one repository area (8 km^2) about each grid point during the next 10,000 years are then calculated (equation (16)). Four such maps are illustrated in Figures 5a–5d. Using $m = 9$ nearest-neighbor volcanoes and data set 1 (Figure 5a), the clustered nature of volcanism in the YMR is captured by the probability surface, with the most significant mode in probability being centered on the Crater Flat Cluster. Modes in probability are also preserved at late Miocene clusters in the eastern part of the YMR, although probabilities of eruption are estimated to be more than 1 order of magnitude lower than in Crater Flat. None of the maps shown indicate increased probability of volcanic eruption in the Sleeping Butte Cluster because of the few vents that compose this cluster. Probability contours on all four maps (Figures 5a–5d) are elongate NNW-SSE, reflecting the overall distribution of Quaternary cones in the CFVZ [*Crowe and Perry*, 1989]. This elongation is more subdued in Figures 5c–5d because of uncertainty in the origin of several aeromagnetic anomalies in Amargosa Valley, which are not included in data set 2.

Application of method 2. Spatial recurrence rate $\lambda_h(x, y)$ (equation (14)) is calculated for the 8 km^2 area about the repository using the same data sets for a range of smoothing constants (Figure 6). For $h = 15$ to 30 km, $\lambda_h(x, y) = 2.3 \times 10^{-4}$ to 6.0×10^{-4} volcanoes per square kilometer (v/km^2) at the repository with a maximum at $h = 17$–20 km for most data sets. At $h < 15$ km the recurrence rate drops with decreasing h to 0 at $h = 8$ km, the approximate distance between Northern Cone and the repository site. Letting $\lambda_t =$
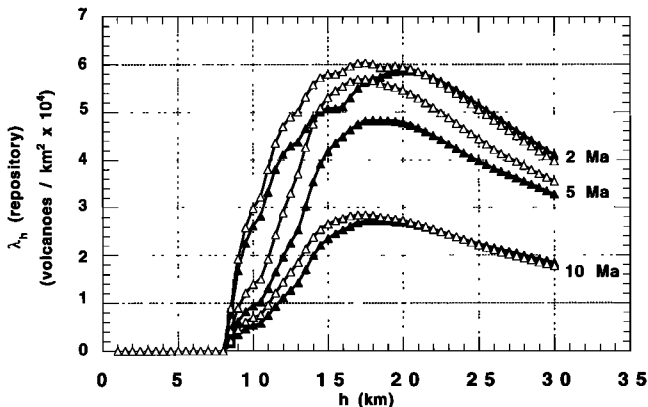

Figure 6. Spatial recurrence rate of volcanism estimated for the location of the proposed repository using method 2, where h is the smoothing constant. Symbols and line labels are as in Figure 3.
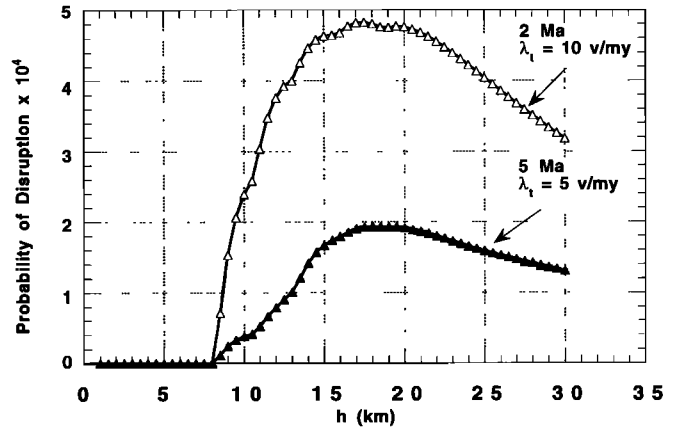

Figure 7. The probability of volcanic disruption of the proposed repository, estimated using method 2, is bounded by the two curves calculated using $a = 8$ km^2, $t = 10,000$ years. Solid triangles, data set 1, including volcanoes <5 Ma and $\lambda_t = 5$ v/m.y. Open triangles, data set 2, including volcanoes formed <2 Ma and $\lambda_t = 10$ v/m.y.

5–10 v/m.y., the probability of volcanic disruption of the repository ($a = 8$ km^2 and $t = 10,000$ years) is calculated in Figure 7 for data set 1 (volcanoes formed <5 Ma) and data set 2 (volcanoes formed <2 Ma), with other calculations falling at intermediate values. Taking 15 km $< h < 25$ km, based on interpretation of the cluster analysis (Figure 2), the probability of volcanic disruption of the repository in 10,000 years is between 1.6×10^{-4} and 4.6×10^{-4}. Maps of the probability of volcanic eruption throughout the region are plotted in Figures 8a and 8b. The clustered nature of volcanism in the YMR is clearly illustrated on these maps, as is the overall NNW trend in post-5 Ma vent distribution. The probability of volcanic eruption drops to zero very close to the log $P[n = 1, a = 8$ km^2, $t = 10,000$ years] $= -4.5$ contour, for $h = 20$ km.

Application of method 3. Spatial recurrence rate $\lambda_r(x, y)$ is calculated at the repository site using (14) where the smoothing constant h is replaced by the distance to the mth nearest-neighbor volcano. The maximum value of $\lambda_r(x, y)$ at the repository is estimated to be 4.2×10^{-4} v/km^2, for data set 2, using volcanoes <2 Ma and the fifth nearest-neighbor (Figure 9). Each of the data sets goes through a maximum, the value of $\lambda_r(x, y)$ at the maximum depending on the number of volcanoes included in the analysis. Data sets of volcanoes <5 Ma and 10 Ma have maxima at the same number of nearest neighbors because the nearest neighbors to the repository are all <5 Ma. Nearly all estimates of $\lambda_r(x, y) > 1 \times 10^{-4}$ v/km^2 (Figure 9). Using volcanoes <5 Ma, the probability of volcanic disruption of the repository site varies from $P[n = 1, a = 8$ km^2, $t = 10,000$ years] $= 5 \times 10^{-5}$ to 1.5×10^{-4}. A maximum probability of 3.3×10^{-4} (Figure 10) is calculated using volcanoes <2 Ma and $\lambda_t = 10$ v/m.y. Maps showing the variation in probability of volcanic eruption across the YMR calculated using $\lambda_r(x, y)$ are plotted in Figures 11a and 11b.

Discussion

The three nonhomogeneous methods are sensitive to basic patterns in cinder cone distribution to varying degrees.
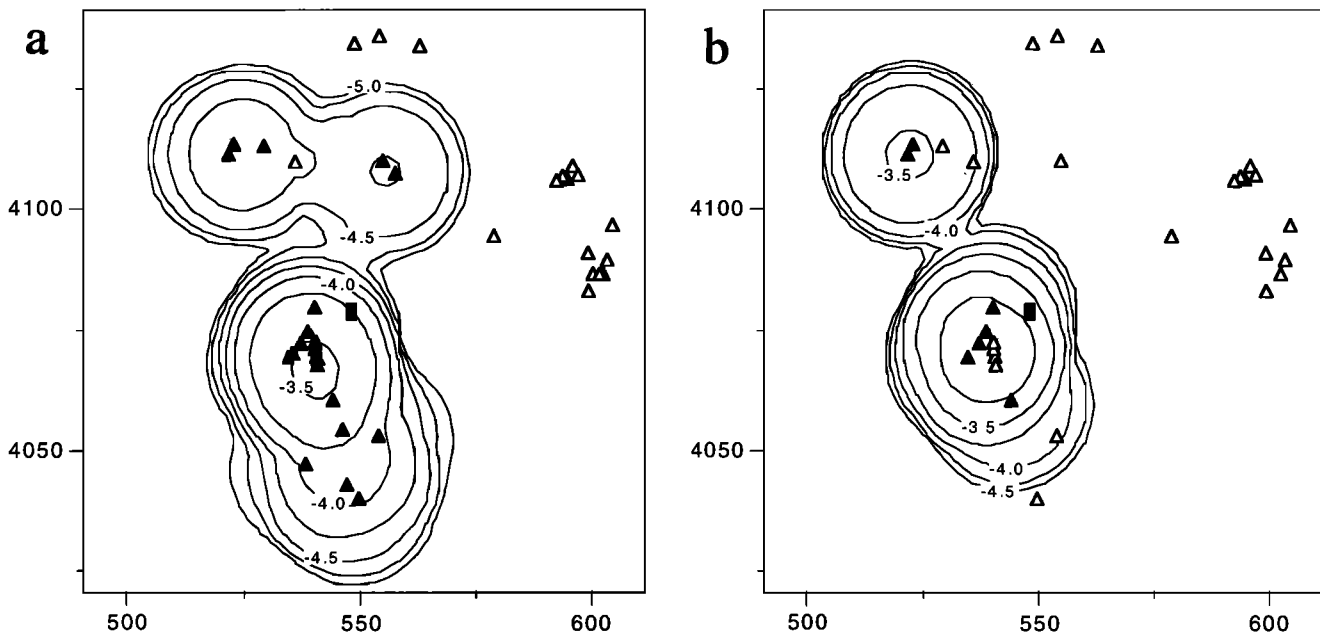
Figure 8. Maps showing the variation in probability of volcanic eruption across the YMR calculated using method 2. As in Figure 5, the logarithm of probability of a volcano forming within a 8 km^2 area during the next 10,000 years is contoured using (a) $h = 20$ km and all volcanoes in data set 1 formed <5 Ma and (b) $h = 20$ km and all volcanoes in data set 2 formed <2 Ma. The contour interval is 0.25 log $(P[N \geq 1, 10,000$ years]) (e.g., -4 is a probability of 1×10^{-4} of a new volcano forming within an 8 km^2 area in 10,000 years), and other symbols are as in Figure 5.

These patterns include shifts in the location of cinder cone volcanism in time, cinder cone clustering, and the presence of vent and regional volcano alignments. These features of areal volcanic fields make nonhomogeneous models very useful for modeling volcano distributions and calculating the probability of future volcanic eruption within these areas.

Comparison of the Three Methods

Method 1 is most sensitive to shifts in the locus of cinder cone volcanism through time because equation (4) incorporates time since volcano formation directly into the recur-

rence rate estimate. Thus, using all postcaldera basalts in the calculation of probability of future volcanic eruption in the YMR, method 1 produces a small mode in probability at late Miocene clusters, but this mode is distinctly smaller than the Crater Flat mode (Figure 5a). Using methods 2 and 3 and the same data, modes at Crater Flat and in late Miocene clusters are of nearly equal amplitude. However, application of method 1 to many other volcanic fields is also more difficult because the ages of all volcanoes in the region must be
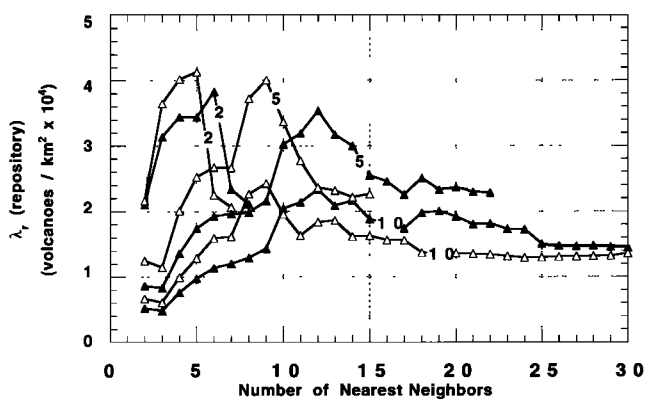

Figure 9. Spatial recurrence rate of volcanism estimated for the location of the proposed repository using method 3. Symbols and line labels are as in Figure 3. The distance to the mth nearest-neighbor volcano is used to calculate normalized distance in the Epanechnikov kernel. Therefore recurrence rate $\lambda_r(x, y)$ varies with the number of nearest neighbors.
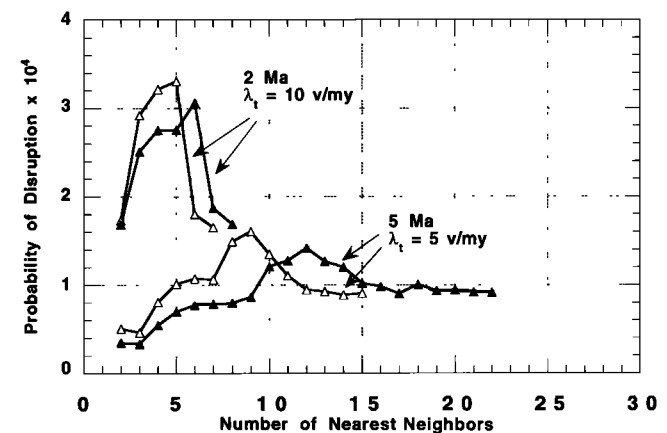
Figure 10. The probability of volcanic disruption of the proposed repository, estimated using method 3, is shown for four curves calculated using $a = 8$ km^2, $t = 10,000$ years. Open triangles, data set 2; solid triangles, data set 1. Calculations using volcanoes formed <2 Ma use $\lambda_t = 10$ v/m.y.; calculations using volcanoes formed <5 Ma use $\lambda_t = 5$ v/m.y.
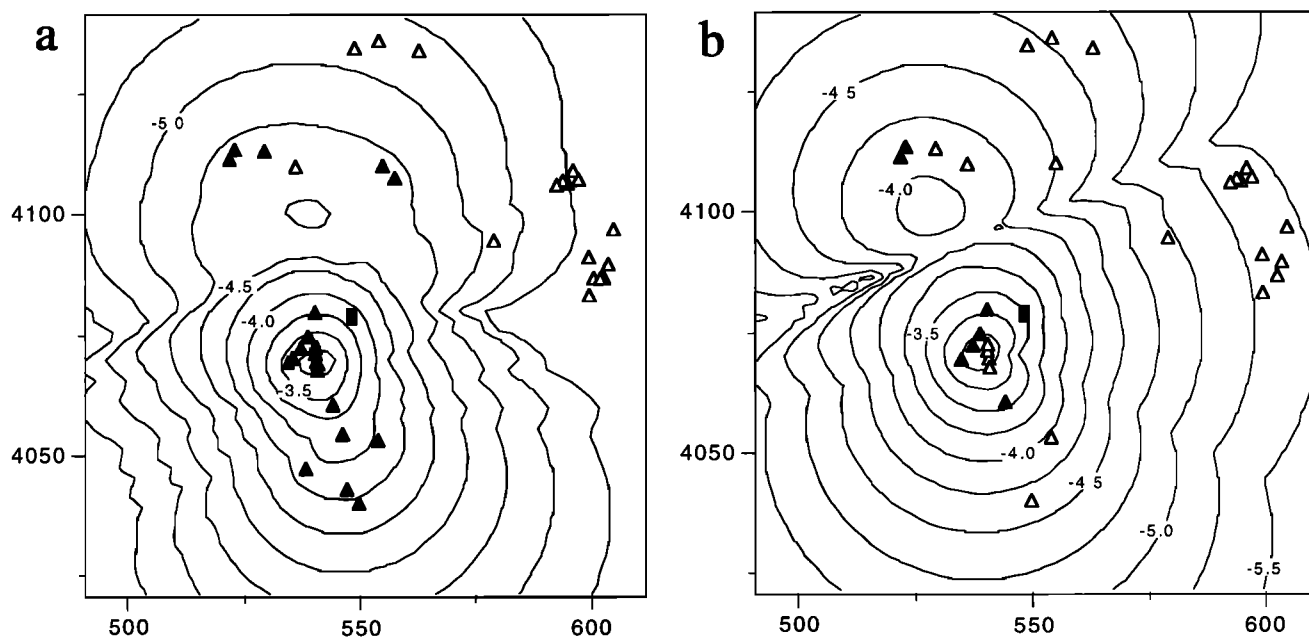
Figure 11. Maps showing the variation in probability of volcanic eruption across the YMR calculated using method 3. As in Figure 5, the logarithm of probability of a volcano forming within a 8 km^2 area during the next 10,000 years is contoured using (a) $m = 12$ nearest neighbors and all volcanoes in data set 1 formed <5 Ma and (b) $m = 5$ nearest neighbors and all volcanoes in data set 2 formed <2 Ma. The contour interval is 0.25 log $(P[N \geq 1, 10,000 \text{ years}])$ (e.g., -4 is a probability of 1×10^{-4} of a new volcano forming within an 8 km^2 area in 10,000 years), and other symbols are as in Figure 5.

known with reasonable precision. In areas where shifts in the locus of volcanism are as temporally distinct as they are in the YMR, methods 2 and 3 are easily adapted by subdividing the volcano data set on the basis of age, as was done for the YMR. Method 2 is least sensitive to shifts in the location of volcanism because the probability of volcanic eruption is zero at distances greater than the smoothing constant if the Epanechnikov kernel is used (equation (13)).

Cinder cone clusters are common and well-documented in basaltic volcanic fields [e.g., *Heming*, 1980; *Connor*, 1990]. This clustering may be the result of various geologic controls on cinder cone emplacement, including the size, distribution, and longevity of partial melt zones, or possibly the heterogeneity of extension rates within the crust [*Heming*, 1980; *Connor*, 1990]. Geological factors such as these suggest a mechanistic basis for application of temporally and spatially nonhomogeneous Poisson probability models. The three nonhomogeneous methods treat clusters using different criteria, with varying results. Method 2 presupposes that volcano density and distance between volcanoes best defines clustering. As a result, for example, method 2 effectively identifies the Sleeping Butte area as a cluster of three volcanoes (Hidden Cone, Little Black Peak, and Thirsty Mountain), in a manner quite consistent with the cluster analysis (Figures 8a and 8b). Methods 1 and 3 presuppose that the number of volcanoes, or volcanic events, is the predominant characteristic defining clusters. Therefore these methods weight rates of volcanic activity between clusters much more heavily than does method 2. For example, methods 1 and 3 do not identify a separate cluster in the Sleeping Butte area, because only three volcanoes define the cluster (e.g., Figures 5a and 11a). Rather, contour lines tend to elongate between the Sleeping Butte Cluster and the

Crater Flat Cluster when recurrence rate is determined using methods 1 and 3, and probability of volcanic eruption in the center of the Crater Flat Cluster is calculated to be comparatively high.

All three methods respond to the presence of regional volcano alignments. In the YMR, the NNW trend of the CFVZ is reflected in the overall shape of the probability surfaces calculated using the three methods (Figures 5b, 8a, and 11a). It is possible to model existing local vent alignments, such as the vent alignments within the Crater Flat Cluster, by decreasing the smoothing constant h in method 2 [*Lutz and Gutmann*, 1995] or decreasing the number of nearest neighbors used in methods 1 and 3. In the case of the YMR, this is achieved by choosing $h < 5$ km or $m \leq 3$ nearest-neighbor volcanoes.

Probability of Volcanic Disruption of the Proposed Yucca Mountain Repository

Volcano clustering in the YMR is statistically significant at the 95% confidence level. Probability models based on a homogeneous Poisson density distribution will overestimate the likelihood of future igneous activity in parts of the YMR far from Quaternary centers and underestimate the likelihood of future igneous activity within and close to Quaternary volcano clusters.

The probability of volcanic disruption of the proposed high-level waste (HLW) repository site, calculated using the three nearest-neighbor methods, is consistently between 1×10^{-4} and 5×10^{-4} in 10,000 years for an 8 km^2 area. This range is close to, or slightly higher than, ranges indicated by most calculations based on homogeneous Poisson models. For example, *Crowe et al.* [1982] propose a range of probability of disruption between 3.3×10^{-6} and 4.7×10^{-4} in

10,000 years, noting that only a "worst case" model leads to probabilities in excess of 1×10^{-4}. Other reported ranges between 1×10^{-6} and 1×10^{-4} in 10,000 years [Crowe et al., 1992a] are close to the probabilities calculated using nearest-neighbor nonhomogeneous models. Differences, especially at the lower bound, arise because the candidate repository site is relatively close to the youngest large volcano cluster in the YMR. More recently, Crowe et al. [1993] proposed a range of models using various area terms and calculated probabilities of disruption between 9×10^{-5} and 2.6×10^{-4} in 10,000 years. "Worst case" homogeneous Poisson models of repository disruption in which structural controls, such as those that may have resulted in the alignment of cinder cones in Crater Flat, are assumed to focus magmatism [Smith et al., 1990; Ho, 1992] and result in probabilities as high as 1×10^{-3} in 10,000 years. The nonhomogeneous models developed here do not support such high probabilities for the candidate repository site, because they do not include this kind of mechanistic control. It is noted that the nonhomogeneous methods do, however, give probabilities as high as 1×10^{-3} in 10,000 years near the center of the Crater Flat Cluster.

The basic agreement between many of these estimates of the probability of volcanic disruption of the proposed repository site must be tempered, however, by a fundamental result of the spatial and spatio-temporal nonhomogeneous techniques developed here. All three nonhomogeneous methods indicate that the proposed repository is positioned on a probability gradient due to its proximity to Crater Flat. Immediately west of the proposed site, the probability of volcanism within the next 10,000 years increases to at least 1×10^{-3} in 10,000 years due to the presence of Quaternary volcanoes in Crater Flat Valley. However, the probability of volcanism within the next 10,000 years decreases east of the proposed repository site. The probability of a new volcano forming within an 8 km^2 area located 20 km east of the site is of the order of 1×10^{-5} in 10,000 years or less. This rapid change in probability, resulting from clustering in volcano distribution, has important implications for the uncertainty associated with the use of probability models. Within 20 km of the proposed site, the probability of volcanism during the next 10,000 years and within a given 8 km^2 area varies by more than 2 orders of magnitude. Given the rapid change in probability across the area, it seems likely that additional geologic information, such as the role of preexisting structure [Smith et al., 1990; McDuffie et al., 1994] or strain rate [Parsons and Thompson, 1991], may alter estimates of the probability of future volcanic activity at the proposed repository site.

The use of the estimates of regional recurrence rate λ_t and the area term for repository disruption a (equations (15) and (16)) and the effect of these assumed values on probability values warrant further discussion. Values of regional recurrence rate of new volcano formation used in the calculations presented here are 5–10 v/m.y. It is a simple matter to recalculate probabilities using different regional recurrence rates. For example, using the range of spatial recurrence rates found using the kernel method (Figure 6), $a = 8$ km^2, and $t = 10,000$ years, the probability of volcanic eruption at the repository site varies from 4.5×10^{-5} to 5.8×10^{-4} for $\lambda_t = 2$ to 12 v/m.y.

Throughout the preceding calculations, λ_t represents the estimated recurrence rate of new volcano formation in the YMR. Some of the geochemical, geomorphological, and geochronological variation present at some YMR Quaternary volcanoes is thought to represent reactivation of these volcanoes after more than 10,000-year quiescence [Wells et al., 1990; Crowe et al., 1992b; Bradshaw and Smith, 1994]. However, results from some other studies appear to contradict this interpretation [Champion, 1991; Turrin et al., 1991], which remains controversial [Whitney and Shroba, 1991; Wells et al., 1991, 1992; Turrin et al., 1992]. Given the possibility of cinder cone reactivation, the range of λ_t of 5–10 v/m.y. may underestimate the rate of volcanic eruptions that will occur in the future in the YMR. However, λ_t is only intended to represent an estimate of the rate of new volcano formation. This is the same as the eruption rate in a monogenetic model but less than the eruption rate in a reactivated volcano model. In the context of volcanic hazards for the proposed repository, the spatially dispersed character of volcanism gives rise to hazards, rather than the reactivation of an existing cinder cone, and λ_t is defined accordingly.

Variation in the repository area term also results in variation in probability estimates. As mentioned above, the total area of the repository is currently estimated to be about 6 km^2. The area radioactive waste occupies within repository depends on design but varies from about 2.3 km^2 for a high thermal load repository to 4.6 km^2 for a lower thermal load repository [Wilson et al., 1994]. Our calculations have been for 8 km^2, which includes the total area of the repository and a buffer zone extending 500 m out from the repository perimeter. This is done in recognition that satellite vents and other direct disruptive effects commonly extend for about 500 m from the central vent. In addition, this buffer accounts for some of the possible deleterious effects of volcanism within a short distance of the repository, such as adverse impact on the hydrological and geochemical setting of the repository. Changing the area term from $a = 8$ km^2 to $a = 4$ km^2 will decrease the range of probability estimates by about a factor of two. Using $a = 4$ km^2 (i.e., low thermal load design) to calculate probability of volcanic disruption implies that volcanism is a point source and that volcanism close to, but not within, a waste storage area has no impact on the isolation of radionuclides. Such assumptions do not seem conservative; consequently, a larger area term is used.

In a similar way, increasing the value of a will increase probability estimates. This is particularly important when probability estimates are made assuming distributed volcanoes represent a single event. This was done in data set 2 by treating NE and SW Little Cones as single events. As a further example, it is possible to consider episodes of cone alignment formation, such as the formation of the Quaternary Crater Flat alignment, to be single events. Of course, this reduces both the total number of volcanic events in the region and the regional recurrence rate λ_t. However, the value of a must be increased to reflect the area impacted by the entire cone alignment.

Experimentation with values of λ_t and a indicates that they have a very limited effect on probability calculations when considered together. Although these variables are important, spatial variation dominates uncertainty in the probability analysis. This salient point illustrates the basic advantages of applying spatially nonhomogeneous methods to volcanic hazards problems.

Conclusions

Nearest-neighbor estimates of spatial and spatio-temporal variation in the recurrence rate of basaltic volcanism can account, to varying degrees, for several basic features of volcano distribution in areal basaltic fields. These features include spatial shifts in the locus of volcanism, the clustering of volcanoes within the field, and the occurrence of volcano alignments. A strength of nearest-neighbor methods is that uncertainty can be estimated, both by mapping variation in the probability surface across the region of interest and through experimentation encompassing the precision and accuracy of geochronological information.

Application of the Hopkins F test and related methods shows that cinder cones cluster in the YMR with greater than 95% confidence. Assuming a regional Quaternary recurrence rate of 5–10 v/m.y., these models estimate probabilities of disruption are generally between 1×10^{-4} and 5×10^{-4} in 10,000 years, in close agreement with some other recent estimates. However, spatial variation in estimated recurrence rate is substantial across the YMR, with the probability of volcanic eruption varying by more than 2 orders of magnitude within 20 km of the proposed repository site. This variation indicates that refinement of models, primarily through the incorporation of additional geological information, may alter these probability estimates significantly.

References

Aherne, W. A., and P. J. Diggle, The estimation of neuronal population density by a robust distance method, *J. Microsc.*, *114*, 285–293, 1978.

Bacon, C. R., Time-predictable bimodal volcanism in the Coso Range, California, *Geology*, *10*, 65–69, 1982.

Bemis, K. G., and D. K. Smith, Production of small volcanoes in the Superswell region of the South Pacific, *Earth Planet. Sci. Lett.*, *118*, 251–262, 1993.

Bradshaw, T. K., and E. I. Smith, Polygenetic Quaternary volcanism at Crater Flat, Nevada, *J. Volcanol. Geotherm. Res.*, *63*, 165–182, 1994.

Braytseva, O. A., I. V. Melekestev, and V. V. Ponomareva, Age divisions of the Holocene volcanic formations of the Tolbachik Valley, in *The Great Tolbachik Fissure Eruption, Geological and Geophysical Data, 1975–1976*, edited by S. A. Fedotov and Y. K. Markhnin, pp. 83–95, Cambridge Univ. Press, New York, 1983.

Byers, F. M., and H. Barnes, Geologic map of the Paiute Ridge Quadrangle, Nye County, Nevada, *U.S. Geol. Surv. Geol. Quad. Map, GQ-577*, 1967.

Byers, F. M., and D. Cummings, Geologic map of the Scrugham Peak Quadrangle, Nye County, Nevada, *U.S. Geol. Surv. Geol. Quad. Map, GQ-695*, 1967.

Byers, F. M., C. L. Rogers, W. J. Carr, and S. J. Luft, Geologic map of the Buckboard Mesa Quadrangle, Nye County, Nevada, *U.S. Geol. Surv. Geol. Quad. Map, GQ-552*, 1966.

Byth, K., and B. D. Ripley, On sampling spatial patterns by distance methods, *Biometrics*, *36*, 279–284, 1980.

Carr, W. J., Regional and structural setting of Yucca Mountain, Southwestern Nevada, and late Cenozoic rates of tectonic activity in part of the southwestern Great Basin, Nevada and California, *U.S. Geol. Surv. Open File Rep.*, *84-854*, 1984.

Carr, W. J., and W. D. Quinlivan, Geologic map of the Timber Mountain Quadrangle, Nye County, Nevada, *U.S. Geol. Surv. Geol. Quad. Map, GQ-503*, 1966.

Champion, D. E., Volcanic episodes near Yucca Mountain as determined by paleomagnetic studies at Lathrop Wells, Crater Flat, and Sleeping Butte, Nevada, in *Second International Conference on High-Level Radioactive Waste Management*, pp. 61–67, Am. Nucl. Soc., Las Vegas, Nev., 1991.

Clark, P. J., and F. C. Evans, On some aspects of spatial pattern in biological populations, *Science*, *121*, 397–398, 1955.

Condit, C. D., L. S. Crumpler, J. C. Aubele, and W. E. Elston, Patterns of volcanism along the southern margin of the Colorado Plateau: The Springerville Field, *J. Geophys. Res.*, *94*, 7,975–7,986, 1989.

Connor, C. B., Cinder cone clustering in the TransMexican volcanic belt: Structural and petrologic implications, *J. Geophys. Res.*, *95*, 19,395–19,405, 1990.

Connor, C. B., and C. D. Condit, Estimating recurrence rate of volcanism in the Springerville volcanic field, Arizona, *Geol. Soc. Am. Abstr. Programs*, *26*, A-115, 1994.

Connor, C. B., C. D. Condit, L. S. Crumpler, and J. C. Aubele, Evidence of regional structural controls on vent distribution: Springerville volcanic field, Arizona, *J. Geophys. Res.*, *97*, 12,349–12,359, 1992.

Cornwall, H. R., Geology and mineral deposits of southern Nye County, Nevada, *Nev. Bur. Mines Geol. Bull.*, *77*, 1972.

Cressie, N. A. C., *Statistics for Spatial Data*, 900 pp., John Wiley, New York, 1991.

Crowe, B. M., Probabilistic volcanic risk assessment, presentation to the Adv. Comm. on Nucl. Waste, Bethesda, Md., 1994.

Crowe, B. M., and F. V. Perry, Volcanic probability calculations for the Yucca Mountain site: Estimation of volcanic rates, in *Proceedings Nuclear Waste Isolation in the Unsaturated Zone, Focus '89*, pp. 326–334, Am. Nucl. Soc., 1989.

Crowe, B., and F. Perry, Preliminary geologic map of the Sleeping Butte Volcanic Centers, *Los Alamos Natl. Lab. Rep., LA-12101-MS*, 1991.

Crowe, B. M., M. E. Johnson, and R. J. Beckman, Calculation of the probability of volcanic disruption of a high-level nuclear waste repository within southern Nevada, USA, *Radioact. Waste Manage. Nucl. Fuel Cycle*, *3*, 167–190, 1982.

Crowe, B. M., D. T. Vaniman, and W. J. Carr, Status of volcanic hazard studies for the Nevada nuclear waste storage investigations, *Los Alamos Natl. Lab. Rep., LA-9325-MS*, 1983.

Crowe, B. M., K. H. Wohletz, D. T. Vaniman, E. Gladney, and N. Bower, Status of volcanic hazard studies for the Nevada nuclear waste storage investigations, *Los Alamos Natl. Lab. Rep., LA-9325-MS*, vol. II, 1986.

Crowe, B. M., C. Harrington, L. McFadden, F. Perry, S. Wells, B. Turrin, and D. Champion, Preliminary geologic map of the Lathrop Wells Volcanic Center, *Los Alamos Natl. Lab. Rep., LA-UR-88-4155*, 1988.

Crowe, B. M., R. Picard, G. Valentine, and F. V. Perry, Recurrence models for volcanic events: Applications to volcanic risk assessment, in *Third International Conference on High-Level Radioactive Waste Management*, pp. 2344–2355, Am. Nucl. Soc., Las Vegas, Nev., 1992a.

Crowe, B., R. Morley, S. Wells, J. Geissman, E. McDonald, L. McFadden, F. Perry, M. Murrell, J. Poths, and S. Forman, The Lathrop Wells volcanic center: Status of field and geochronology studies, in *Third International Conference on High-Level Radioactive Waste Management*, pp. 1997–2013, Am. Nucl. Soc., Las Vegas, Nev., 1992b.

Crowe, B. M., F. V. Perry, G. A. Valentine, P. C. Wallmann, and R. Kossik, Simulation modeling of the probability of magmatic disruption of the potential Yucca Mountain site, in *Proceedings, Site Characterization and Model Validation, Focus '93*, pp. 182–191, Am. Nucl. Soc., Las Vegas, Nev., 1993.

Department of Energy (DOE), Site Characterization Plan: Yucca Mountain Site, Nevada Research and Development Area, Nevada, *Rep. DOE/RW-0199*, Off. of Radioactive Waste Manage., Washington, D. C., 1988.

Diggle, P. J., A note on robust density estimation for spatial point patterns, *Biometrika*, *64*, 91–95, 1977.

Diggle, P. J., On parameter estimation for spatial point patterns, *J. R. Stat. Soc. B*, *40*, 178–181, 1978.

Diggle, P. J., A kernel method for smoothing point process data, *Appl. Stat.*, *34*, 138–147, 1985.

Dohrenwend, J. C., L. D. MacFadden, B. D. Turrin, and S. G. Wells, K-Ar dating of the Cima volcanic field, eastern Mojave Desert, California: Late Cenozoic volcanic history and landscape evolution, *Geology*, *12*, 163–167, 1984.

Draper, G., Z. Chen, M. Conway, C. B. Connor, and C. D. Condit, Structural control on magma pathways in the upper crust: Insights from the San Francisco volcanic field, Arizona, *Geol. Soc. Am. Abstr. Programs*, *26*, A-115, 1994.

Duffield, W. A., C. R. Bacon, and G. B. Dalrymple, Late Cenozoic volcanism, geochronology, and structure of the Coso Range, Inyo County, California, *J. Geophys. Res.*, *85*, 2381–2404, 1980.

Eichelberger, J. C., and R. Gooley, Evolution of silicic magma chambers and their relationship to basaltic volcanism, in *The Earth's Crust*, *Geophys. Monogr. Ser.*, vol. 20, edited by J. G. Heacock, pp. 57–77, AGU, Washington, D. C., 1977.

Ekren, E. B., R. E. Anderson, P. P. Orkild, and E. N. Hinrichs, Geologic map of the Silent Butte Quadrangle, Nye County, Nevada, *U.S. Geol. Surv. Geol. Quad. Map*, *GQ-493*, 1966.

Faulds, J. E., J. W. Bell, D. L. Feuerbach, and A. R. Ramelli, Geologic map of the Crater Flat Area, Nevada, *Nev. Bur. Mines Geol. Map*, *101*, 1994.

Foland, K. A., and S. C. Bergman, Temporal and spatial distribution of basaltic volcanism in the Pancake and Reveille ranges north of Yucca Mountain, in *Third International Conference on High-Level Radioactive Waste Management*, pp. 2366–2371, Am. Nucl. Soc., Las Vegas, Nev., 1992.

Hasenaka, T., and I. S. E. Carmichael, The cinder cones of Michoacán-Guanajuato, central Mexico: Their age, volume, distribution, and recharge rate, *J. Volcanol. Geotherm. Res.*, *25*, 195–204, 1985.

Heizler, M. T., W. C. McIntosh, F. V. Perry, and B. M. Crowe, ^{40}Ar/^{39}Ar results of incompletely degassed sanidine: Age of Lathrop Wells volcanism, *U.S. Geol. Surv. Circ.*, *1107*, 133, 1994.

Heming, R. F., Patterns of Quaternary basaltic volcanism in the northern North Island, New Zealand, *N. Z. J. Geol. Geophys.*, *23*, 335–344, 1980.

Hinrichs, E. N., R. D. Krushensky, and S. J. Luft, Geologic map of the Ammonia Tanks Quadrangle, Nye County, Nevada, *U.S. Geol. Surv. Geol. Quad. Map*, *GQ-638*, 1967.

Ho, C.-H., Time trend analysis of basaltic volcanism at the Yucca Mountain site, *J. Volcanol. Geotherm. Res.*, *46*, 61–72, 1991.

Ho, C.-H., Risk assessment for the Yucca Mountain high-level nuclear waste repository site: Estimation of volcanic disruption, *Math. Geol.*, *24*, 347–364, 1992.

Ho, C.-H., E. I. Smith, D. L. Feuerbach, and T. R. Naumann, Eruptive probability calculation for the Yucca Mountain site, USA: Statistical estimation of recurrence rates, *Bull. Volcanol.*, *54*, 50–56, 1991.

Kane, M. F., and R. E. Bracken, Aeromagnetic map of Yucca Mountain and surrounding regions, southwest Nevada, *U.S. Geol. Surv. Open File Rep.*, *83-616*, 19 pp., 1983.

Kear, D., Volcanic alignments north and west of New Zealand's central volcanic region, *N. Z. J. Geol. Geophys.*, *7*, 24–44, 1964.

Langenheim, V. E., K. S. Kirchoff-Stein, and H. W. Oliver, Geophysical investigations of buried volcanic centers near Yucca Mountain, southwestern Nevada, in *Fourth International Conference on High-Level Radioactive Waste Management*, pp. 1840–1846, Am. Nucl. Soc., Las Vegas, Nev., 1993.

Lutz, T. M., An analysis of the orientations of large scale crustal structures: A statistical approach based on areal distributions of pointlike features, *J. Geophys. Res.*, *91*, 421–434, 1986.

Lutz, T. M., and J. T. Gutmann, An improved method of determining and characterizing alignments of pointlike features and its implications for the Pinacate volcanic field, Sonora, Mexico, *J. Geophys. Res.*, in press, 1995.

Magus'kin, M. A., V. B. Enman, and V. S. Tselishchev, Changes in the height, volume, and shape of the New Tolbachik volcanoes of the Northern Breakthrough, in *The Great Tolbachik Fissure Eruption, Geological and Geophysical data, 1975–1976*, edited by

S. A. Fedotov and Y. K. Markhnin, pp. 307–315, Cambridge Univ. Press, New York, 1983.

Margulies, T., L. Lancaster, N. Eisenberg, and L. Abramson, Probabilistic analysis of magma scenarios for assessing geologic waste repository performance, *Rep. 92-WA/SAF-11*, Am. Soc. of Mech. Eng., New York, 1992.

McBirney, A. R., Volcanology, in *Techniques for Determining Probabilities of Geologic Events and Processes*, *Stud. Math. Geol.*, no. 4, edited by R. L. Hunter and C. J. Mann, pp. 167–184, Oxford Univ. Press, New York, 1992.

McDuffie, S., C. B. Connor, and K. D. Mahrer, A simple model of fault-dike interaction, *Eos Trans. AGU*, *75*(16), Spring Meet. suppl., 345, 1994.

Nakamura, K., Volcanoes as possible indicators of tectonic stress orientation—Principles and proposal, *J. Volcanol. Geotherm. Res.*, *2*, 1–16, 1977.

Noble, D. C., R. D. Krushensky, E. J. McKay, and J. R. Ege, Geologic map of the Dead Horse Flat Quadrangle, Nye County, Nevada, *U.S. Geol. Surv. Geol. Quad. Map*, *GQ-614*, 1967.

Parsons, T., and G. A. Thompson, The role of magma overpressure in suppressing earthquakes and topography: worldwide examples, *Science*, *253*, 1399–1402, 1991.

Perry, F. M., Update on characterization of volcanic features, presentation to the Adv. Commit. Nucl. Waste, Bethesda, Md., 1994.

Poths, J., and B. M. Crowe, Surface exposure ages and noble gas components of volcanic units at the Lathrop Wells volcanic center, Nevada, *Eos Trans. AGU*, *73*(43), Fall Meet. suppl., 610, 1992.

Poths, J., F. Perry, and B. M. Crowe, ^{3}He surface exposure ages at the Lathrop Wells, NV, volcanic center, *U.S. Geol. Surv. Circ.*, *1107*, 255, 1994.

Ripley, B. D., Modelling spatial patterns, *J. R. Stat. Soc. B*, *39*, 172–212, 1977.

Ripley, B. D., Spatial statistics, in *Wiley Series in Probability and Mathematics*, 252 pp., John Wiley, New York, 1981.

Sawyer, D. R., R. J. Fleck, M. A. Lanphere, R. G. Warren, D. E. Broxton, and M. R. Hudson, Episodic caldera volcanism in the Miocene southwestern Nevada volcanic field: Revised stratigraphic framework, ^{40}Ar/^{39}Ar geochronology, and implications for magmatism and extension, *Geol. Soc. Am. Bull.*, *106*, 1304–1318, 1994.

Settle, M., The structure and emplacement of cinder cone fields, *Am. J. Sci.*, *279*, 1089–1107, 1979.

Sheridan, M. F., A Monte Carlo technique to estimate the probability of volcanic dikes, in *Third International Conference on High-Level Radioactive Waste Management*, pp. 2033–2038, Am. Nucl. Soc., Las Vegas, Nev., 1992.

Silverman, B. W., *Density Estimation for Statistics and Data Analysis*, 175 pp., Chapman and Hall, New York, 1986.

Sinnock, S., and R. G. Easterling, Empirically determined uncertainty in potassium-argon ages for Plio-Pleistocene basalts from Crater Flat, Nye County, Nevada, *Sandia Natl. Lab. Rep.*, *SAND 82-2441*, 1983.

Smith, E. I., T. R. Naumann, D. L. Feuerbach, and J. E. Faulds, The area of most recent volcanism near Yucca Mountain, Nevada: Implications for volcanic risk assessment, in *International Meeting on High-Level Radioactive Waste Management*, pp. 81–90, Am. Nucl. Soc., Las Vegas, Nev., 1990.

Späth, H., *Clustering Algorithms*, 226 pp., John Wiley, New York, 1980.

Swadley, W. C., and W. J. Carr, Geologic map of the Quaternary and Tertiary deposits of the Big Dune Quadrangle, Nye County, Nevada, and Inyo County, California, *U.S. Geol. Surv. Misc. Invest. Ser. Map*, *I-1767*, 1987.

Takada, A., The influence of regional stress and magmatic input on styles of monogenetic and polygenetic volcanism, *J. Geophys. Res.*, *99*, 13,563–13,574, 1994.

Tanaka, K. L., E. M. Shoemaker, G. E. Ulrich, and E. W. Wolfe, Migration of volcanism in the San Francisco volcanic field, Arizona, *Geol. Soc. Am. Bull.*, *97*, 129–141, 1986.

Tokarev, P. I., Calculation of the magma discharge, growth in the height of the cone and dimensions of the feeder channel of Crater I in the Great Tolbachik Fissure Eruption, July 1975, in *The Great Tolbachik Fissure Eruption, Geological and Geophysical data,*

1975–1976, edited by S. A. Fedotov and Ye. K. Markhnin, pp. 27–35, Cambridge Univ. Press, New York, 1983.

Tschanz, C. M., and E. H. Pampeyan, Geology and mineral deposits of Lincoln County, Nevada, *Nev. Bur. Mines Geol. Bull.*, *73*, 1970.

Turrin, B., New high-precision ^{40}Ar/^{39}Ar step heating results from basalts near Yucca Mountain, paper presented at Panel on Structural Geology and Engineering Meeting on Volcanism, U.S. Nucl. Waste Tech. Rev. Board, Las Vegas, Nev., 1992.

Turrin, B. D., J. C. Dohrenwend, R. E. Drake, and G. H. Curtis, K-Ar ages from the Cima volcanic field, eastern Mojave Desert, California, *Isochron West*, *44*, 9–16, 1985.

Turrin, B. D., D. Champion, and R. J. Fleck, ^{40}Ar/^{39}Ar age of the Lathrop Wells volcanic center, Yucca Mountain, Nevada, *Science*, *253*, 654–657, 1991.

Turrin, B. D., D. Champion, and R. J. Fleck, Measuring the age of the Lathrop Wells volcanic center at Yucca Mountain: Response, *Science*, *257*, 556–558, 1992.

Vaniman, D. T., and B. M. Crowe, Geology and petrology of the Basalts of Crater Flat: Applications to volcanic risk assessment for the nuclear waste storage investigations, *Los Alamos Natl. Lab. Rep.*, *LA-8845-MS*, 1981.

Vaniman, D. T., B. M. Crowe, and E. S. Gladney, Petrology and geochemistry of Hawaiite lavas from Crater Flat, Nevada, *Contrib. Mineral. Petrol.*, *80*, 341–357, 1982.

Wadge, G., and A. Cross, Quantitative methods for detecting aligned points: An application to the vents of the Michoacán-Guanajuato volcanic field, Mexico, *Geology*, *16*, 815–818, 1988.

Wadge, G., P. A. V. Young, and I. J. McKendrick, Mapping lava flow hazards using computer simulation, *J. Geophys. Res.*, *99*, 489–504, 1994.

Wells, S. G., L. D. McFadden, C. E. Renault, and B. M. Crowe, Geomorphic assessment of late Quaternary volcanism in the Yucca Mountain area, southern Nevada: Implications for the proposed high-level radioactive waste repository, *Geology*, *18*, 549–553, 1990.

Wells, S. G., L. D. McFadden, C. E. Renault, and B. M. Crowe, Reply to Whitney and Shroba's comment on "Geomorphic assessment of late Quaternary volcanism in the Yucca Mountain area, southern Nevada: Implications for the proposed high-level radioactive waste repository," *Geology*, *18*, 661–662, 1991.

Wells, S. G., B. M. Crowe, and L. D. McFadden, Measuring the age of the Lathrop Wells Volcanic Center at Yucca Mountain: Comment, *Science*, *257*, 555–556, 1992.

Whitney, J. W., and R. R. Shroba, Comment on "Geomorphic assessment of late Quaternary volcanism in the Yucca Mountain area, southern Nevada: Implications for the proposed high-level radioactive waste repository," *Geology*, *18*, 661, 1991.

Wilson, M. L., et al., Total-system performance assessment for Yucca Mountain—SNL second iteration (TSPA-1993), *Sandia Natl. Lab. Rep.*, *SAND93-2675*, 1994.

Zoback, M. L., State of stress in the northern Basin and Range Province, *J. Geophys. Res.*, *94*, 7105–7128, 1989.

Zreda, M. G., F. M. Phillips, P. W. Kubik, P. Sharma, and D. Elmore, Cosmogenic ^{36}Cl dating of a young basaltic eruption complex, Lathrop Wells, Nevada, *Geology*, *21*, 57–60, 1993.

C. B. Connor and B. E. Hill, Center for Nuclear Waste Regulatory Analyses, Southwest Research Institute, Bldg. 189, 6220 Culebra Road, San Antonio, TX 78238-5166. (e-mail: cconnor@swri.edu)